



THE UNIVERSITY *of* EDINBURGH

Edinburgh Research Explorer

Major icesheet change in the Weddell Sea Sector of West Antarctica over the last 5000 years

Citation for published version:

Siegert, M, Kingslake, J, Ross, N, Whitehouse, PL, Woodward, J, Jamieson, SSR, Bentley, MJ, Winter, K, Wearing, M, Hein, A, Jeofry, H & Sugden, D 2019, 'Major icesheet change in the Weddell Sea Sector of West Antarctica over the last 5000 years', *Reviews of Geophysics*, vol. 57, pp. 1197-1223.
<https://doi.org/10.1029/2019RG000651>

Digital Object Identifier (DOI):

[10.1029/2019RG000651](https://doi.org/10.1029/2019RG000651)

Link:

[Link to publication record in Edinburgh Research Explorer](#)

Document Version:

Peer reviewed version

Published In:

Reviews of Geophysics

General rights

Copyright for the publications made accessible via the Edinburgh Research Explorer is retained by the author(s) and / or other copyright owners and it is a condition of accessing these publications that users recognise and abide by the legal requirements associated with these rights.

Take down policy

The University of Edinburgh has made every reasonable effort to ensure that Edinburgh Research Explorer content complies with UK legislation. If you believe that the public display of this file breaches copyright please contact openaccess@ed.ac.uk providing details, and we will remove access to the work immediately and investigate your claim.



Late Holocene Glacial History of the Weddell Sea Sector of the West Antarctic Ice Sheet

Martin J Siegert¹, Jonny Kingslake², Neil Ross³, Pippa L. Whitehouse⁴, John Woodward⁵, Stewart S R Jamieson⁴, Michael J Bentley⁴, Kate Winter⁵, Martin Wearing², Andrew S Hein⁶, Hafeez Jeofry¹, David E Sugden⁶

1. *Grantham Institute and Department of Earth Science and Engineering, Imperial College London, London SW7 2AZ, UK*
2. *Lamont-Doherty Earth Observatory, Columbia University, Palisades, NY, 10964, USA*
3. *School of Geography, Politics and Sociology, Newcastle University, Newcastle upon Tyne, NE1 7RY, UK*
4. *Department of Geography, Durham University, South Road, Durham, DH1 3LE, UK*
5. *Department of Geography and Environmental Sciences, Faculty of Engineering and Environment, Northumbria University, Newcastle upon Tyne, NE1 8ST, UK*
6. *School of GeoSciences, University of Edinburgh, Drummond Street, Edinburgh, EH8 9XP, UK*

Abstract

Until recently, little was known about the Weddell Sea sector of the West Antarctic Ice Sheet. In the last 10 years, a variety of expeditions and numerical modelling experiments have improved knowledge of its glaciology, glacial geology, and tectonic setting. Two of the sector's largest ice streams rest on a steep reverse-sloping bed yet, despite being vulnerable to change, satellite observations show contemporary stability. There is clear evidence for major ice-sheet reconfiguration in the last few thousand years, however. Knowing precisely how the ice sheet has changed in the past, and when, would allow us to better understand whether it is now at risk. Two competing hypotheses have been established for this glacial history. In one, the ice sheet retreated and thinned progressively from its Last Glacial Maximum position. Retreat stopped at, or very near, the present position in the Late Holocene. Alternatively, in the Late Holocene the ice sheet retreated significantly upstream of the present grounding line, and then advanced to the present location due to glacial isostatic adjustment, and ice-shelf and ice rise buttressing. Both hypotheses point to data and theory in their support, yet neither has been unequivocally tested or falsified. Here, we review geophysical evidence to determine how each hypothesis has been formed, where there are inconsistencies in the respective glacial histories, how they may be tested or reconciled, and what new evidence is required to reach a common model for the Late Holocene ice sheet history of the Weddell Sea sector of West Antarctica.

Plain Language Summary

The West Antarctic Ice Sheet is vulnerable to climate and ocean warming because it rests on a bed more than 2 km below sea level in some places. Understanding how this ice sheet has changed in the recent past guides our appreciation of how it will change in the near future. Getting such information requires measurement of: (1) structures in the ice that are influenced by former ice-sheet change; (2) the age of sediment on surfaces exposed above the ice now but that were previously covered; and (3) numerical modelling of ice-sheet processes to understand what change is realistic. The ice sheet was certainly a lot bigger at the ice age, 20,000 years ago, but two alternative histories exist on how it shrank to today's size. In one, the ice sheet gets smaller gradually over time and, in the other, the ice sheet becomes smaller than today before it expands and comes to rest. Arriving at a single history for the ice sheet may allow us to better understand whether to expect change to occur here in future and how it may happen.

Key Points

- The Weddell Sector has experienced major change since the Late Holocene.
- It is unclear whether the ice sheet gradually shrank to its modern size from its full-glacial state, or became smaller here and then regrew.
- Targeted geophysics, dating of buried and exposed surfaces, and sediment drilling, may resolve the inconsistencies in glacial history.

57	Glossary of terminology
58	LGM Last Glacial Maximum, around 20,000 years ago
59	Holocene The Last ~10,000 years of Earth history
60	BIR, HIR, KIR Bungenstock, Henry and Korff ice rises
61	WS Weddell Sea
62	WAIS West Antarctic Ice Sheet
63	EAIS East Antarctic Ice Sheet
64	SWSE Southern Weddell Sea Embayment
65	RIS, IIS, MIS, FIS Rutford, Institute, Möller and Foundation ice streams
66	RES Radio-echo Sounding
67	GIA Glacial Isostatic Adjustment
68	Al, Be, C Aluminium, Beryllium, Carbon
69	GPS Global Positioning System
70	ka thousand years ago
71	Ma million years ago
72	Scenario MAX Maximum LGM extent of ice
73	Scenario MIN Minimum LGM extent of ice
74	Scenario A Gradual retreat of ice in the Holocene from LGM values
75	Scenario B Holocene retreat upstream of today's grounded limit with subsequent ice
76	expansion
77	MISI Marine Ice Sheet Instability - associated with ice retreat across retrograde bed slope
78	below sea level
79	GL Grounding Line, separating the grounded ice sheet and the floating ice shelf (also
80	referred to as the Grounding Zone, as the transition between floating and grounded ice is
81	rarely sharp)
82	Nunatak exposed pinnacle of rock surrounding by thick ice
83	exposure age the time since material has been uncovered
84	ice rise a dome of ice with higher elevation and slower flow speed than surrounding ice
85	
86	

87 Introduction

88 Quantification of future sea-level rise is hindered by uncertainty regarding how the world's
89 polar ice sheets will change under global warming scenario [IPCC, 2013]. While satellite
90 observations have allowed an appreciation of how ice sheets are changing today (and over
91 the last 40 years) [Shepherd et al., 2018; Rignot et al., 2018] key to understanding how they
92 will change in the future is knowledge of their most recent significant alterations. However,
93 this knowledge requires that we have proficient geophysical measurements of ice sheet form
94 and flow, and past change, in the most vulnerable ice-sheet regions.

95 The Weddell Sea (WS) sector of the West Antarctic Ice Sheet (WAIS) (Figure 1) was, until
96 10 years ago, one of the poorest understood regions of Antarctica. Since then there has
97 been a plethora of airborne and ground based geophysics (including ice-penetrating radar
98 and solid earth measurements), glacial geological and geomorphological analysis
99 (cosmogenic nuclide dating analysis of exposed surfaces) and numerical modelling activities
100 (of ice and earth). An area of focus for research within the WS sector has been the Southern
101 WS embayment (SWSE), involving the area including the Rutford, Institute, Möller and
102 Foundation ice streams (RIS, IIS, MIS and FIS) and the Bungenstock, Henry and Korff ice
103 rises (BIR, HIR and KIR). Investigations here point to substantial change to this sector of the
104 WAIS during the Holocene. However, the details of this change are open to debate, with
105 some considering progressive monotonic retreat of the ice-sheet margin from a Last Glacial
106 Maximum (LGM) position at the edge of the continental shelf, with associated ice flow
107 reconfiguration [Hillenbrand et al., 2014], and others suggesting the grounding line retreated
108 significantly inland of its present position, with subsequent ice-sheet readvance and flow
109 reconfiguration [Siebert et al., 2013; Bradley et al., 2015; Kingslake et al., 2018]. There is
110 also a lack of consensus on the timing of this change, due to a shortage of absolute dating
111 control, and presently no synthesis of the ideas published. Here, by reviewing the available
112 information, we establish how each of the glacial histories are supported with data and
113 models, where evidence is contradictory, and what new data might be needed to reach a
114 single consistent glacial history for the region. This is important, because the SWSE could
115 be at a physical threshold of major change, with two ice streams sitting atop a major
116 reversing bed slope, and several ice streams grounded far (~2 km) below sea level [Ross et
117 al., 2012; Jeofry et al., 2018a]. This makes them potentially unstable to perturbations in
118 grounding line position [Wright et al., 2014]. Conversely, three large ice rises and a set of ice
119 rumples (slow-moving regions of grounded ice) sit within the Ronne-Filchner Ice Shelf,
120 providing pinning points for ice-shelf buttressing to these ice streams, which tends to
121 stabilize grounding lines [Matsuoka et al., 2015]. By understanding past ice sheet change in
122 this region, in particular assessing whether the ice sheet has retreated or expanded recently
123 in the Holocene and if it is currently experiencing ongoing change, we can better evaluate
124 how the ice sheet may change in the future by determining whether it is susceptible to
125 further ice retreat, or whether recent expansion, driven perhaps by isostatic uplift of the solid
126 Earth, has led to its stability.

127 The recent literature has been developed as a consequence of several geophysical
128 campaigns and techniques. It has benefitted from airborne and ground based ice-penetrating
129 radar, solid earth lithospheric measurements, cosmogenic nuclide analysis, and numerical
130 ice sheet and solid earth modelling. This review thus draws together a variety of geophysical
131 techniques, and integrates and evaluates the measurements and data from these

techniques to understand the glacial history of this enigmatic region of West Antarctica, during the Holocene period.

2. The Southern Weddell Sea Embayment of the WAIS

The SWSE was the subject of a major aerogeophysical survey in 2010-11 [Ross *et al.*, 2012], revealing the ~2 km deep Robin Subglacial Basin immediately upstream of present-day grounding lines. The revised bed was used in ice-sheet modelling to quantify the sensitivity of this part of the ice sheet to ocean and atmospheric forcing [Wright *et al.*, 2014]. Further geophysical surveying of the region, both by air and on ice, has been undertaken by the British Antarctic Survey since Bedmap2 [Rosier *et al.*, 2018; Winter *et al.*, 2018] and NASA's Operation IceBridge (operated by the CReSIS and the University of Kansas (<https://www.cresis.ku.edu/>)). This has improved our knowledge of the land surface beneath the ice sheet, leading to a revised digital bed elevation model (DEM) of the region [Jeofry *et al.*, 2018a]. Immediately to the north of the region targeted by these studies, two ground-based geophysics traverses of the Southern Ronne Ice Shelf and several of the regions ice rises was conducted in 2013-15, also by the British Antarctic Survey [Kingslake *et al.*, 2015].

2. 1 Geology and topography

Geophysical data reveal that the WS sector encompasses thinned crust extending ~1200 km from the continental slope south to the Ellsworth-Whitmore Mountains tectonic block [Jordan *et al.*, 2013]. The Ellsworth-Whitmore Mountains tectonic block [Dalziel and Elliot, 1982] is bounded on its north side by the WS embayment and the Antarctic Peninsula. IIS and MIS flow north from the block into the Ronne-Filchner Ice Shelf. Several isolated nunataks (e.g., Pirrit Hills, Martin and Nash Hills, Pagano Nunatak) that protrude above the ice surface across the WS sector, result from a ~5 – 10 km thick Jurassic granite intrusion dated to ~175 Ma [Jordan *et al.*, 2013]. The Pagano Shear Zone is a major crustal shear boundary with a dominant NW - SE trend [Curtis, 2001; Jordan *et al.*, 2013]. It is located across the region of the Transitional and Marginal Basins, where it is overlain with highly deformed Palaeozoic metasediments (512 – 250 Ma). Aeromagnetic anomalies indicate that Palaeozoic metasediments and ~13 km thick Cambrian igneous rocks overlie the Proterozoic basement (2500 – 541 Ma) in several sectors of the Ellsworth Domain [Jordan *et al.*, 2013].

The bed topography of the WS is both rough (over mountains and exposed bedrock) and smooth (across sediment-filled regions) [Bingham and Siegert, 2007]. The deepest parts of the Robin Subglacial Basin (Figure 1a) are anomalously rough, marking the edge of a sedimentary drape [Siegert *et al.*, 2016], whilst the subglacial topography of the region between the Robin Subglacial Basin and the Pirrit and Martin-Nash Hills is relatively flat, smooth and gently sloping. Rose *et al.* [2015] defined this flat region as a bedrock planation surface: a geomorphological feature that might be attributable by marine and/or fluvial erosion [Sugden and Jamieson, 2018]. A series of large sub-parallel subglacial bed channels, thought to have been formed by the flow of basal water, lie between the MIS and Filchner Ice Stream (Figure 1b) [Rose *et al.*, 2014]. As these channels are presently located beneath slow moving and cold-based ice the channels must be ancient; possibly formed at a time when the ice sheet was temperate and surface melting was prevalent in West

Antarctica. Field evidence and modelling suggests that such conditions may have last existed in the mid-Miocene [Sugden *et al.*, 2017]. In other parts of the WS sector higher bed elevations allow the Ronne Filchner Ice Shelf to ground, creating ice surface features known as ice rises and rumpled [Matsuoka *et al.*, 2015], the largest of which include the BIR and HIR (Figure 1).

2.2 Glaciology

The SWSE is composed of three major ice-sheet outlets (Figure 1); the IIS, MIS and FIS, respectively, feeding ice to the Ronne-Filchner Ice Shelf, the second largest ice shelf in Antarctica after the Ross Ice Shelf. Subglacial topography and geology control the position and dynamics of these ice streams (the downstream ice shelf is also a major control on dynamics and GL position). The IIS and MIS grounding lines sit atop a steep reverse bed slope [Ross *et al.*, 2012], similar in scale to that measured for upstream Thwaites Glacier. The bed slopes inland to a ~1.8 km deep basin (the Robin Subglacial Basin), which is divided into two sections, with few obvious significant ice-sheet pinning points [Ross *et al.*, 2012].

The IIS has three tributaries to the south and west of the Ellsworth Mountains, occupying the Horseshoe Valley, Independence Trough and Ellsworth Trough [Bamber *et al.*, 2000; Ross *et al.*, 2014; Winter *et al.*, 2015]. The Horseshoe Valley Trough, around 20 km wide and 1.3 km below sea level at its deepest point, is located downstream of the steep mountains of the Heritage Range. A subglacial ridge is located between the mouth of the Horseshoe Valley Trough and the main trunk of the IIS [Winter *et al.*, 2015]. The Independence Trough is subparallel to Horseshoe Valley Trough, separated by the 1.4 km high of the Independence Hills. The trough is ~22 km wide and over 1 km below sea level at its deepest point. It is characterized by two distinctive plateaus (~6 km wide each) on either side of the trough, which are aligned alongside the main trough axis. Presently, ice flows eastward through the Independence Trough for ~54 km before it shifts to a northward direction, where the trough widens to 50 km at its connection with the main IIS. The Ellsworth Trough [Ross *et al.*, 2014] is aligned with the Independence Trough; both are orthogonal to the orientation of the Amundsen – Weddell ice divide, dissecting the Ellsworth Subglacial Highlands northwest to southeast. The Ellsworth Trough is considered to be the largest and deepest trough-controlled tributary of the IIS [Ross *et al.*, 2014; Winter *et al.*, 2015], measuring ~34 km in width and ~260 km in length. At its deepest point, the Ellsworth Trough extends ~2 km below sea level. The trough contains the ~15 – 20 km long Ellsworth Subglacial Lake [Siebert *et al.*, 2004a, 2012; Woodward *et al.*, 2010]. The Ellsworth Trough is intersected by several smaller valleys aligned perpendicularly to the main axis, which are relic landforms from a past small dynamic ice mass (predating the WAIS in its present configuration) [Ross *et al.*, 2014].

The MIS is smaller than IIS, and is supplied by ice from the upstream IIS tributary (Mouginot *et al.* 2017). A bifurcation south of the BIR sends most of the ice into the IIS trunk, and a smaller fraction into the MIS. The shear margins of the two ice streams interact differently with the BIR. The IIS-BIR shear margin is controlled thermally; the IIS bed is wet whilst the BIR is frozen at its base [Siebert *et al.*, 2016]. The MIS-BIR margin is controlled tectonically

by the Pagano Shear Zone (see below); which has created a subglacial trough, currently occupied by the MIS.

The trunk of the FIS occupies a very deep (~2km) trench, fed by ice from both the WAIS (via an upstream tributary of the FIS) and the East Antarctic Ice Sheet (EAIS) (i.e., through Academy Glacier). The grounding line of the FIS rests on a horizontal bed and has been shown to oscillate across the bed by ~20 km as a consequence of tidal forcing, where the trunk of the ice stream is floated at high tide and grounded at low tide [Jeofry *et al.*, 2018b].

The flow of subglacial water is critical to the ice dynamics of the WS sector of the WAIS. Jeofry *et al.* [2018b] calculated the pathways of basal water flow using recently constructed bed and surface DEMs. This study reveals how water flows beneath the tributaries and into the trunks of the ice streams. It also shows how each of the ice streams interacts distinctly with this water. For IIS, the greatest surface ice flow velocities are recorded across a well-defined sedimentary drape, which is predominantly fed by water from the upstream IIS catchment, which also feeds water downstream to the Robin Subglacial Basin, where it exits the ice sheet as a point-source, etching a channel upwards into the ice shelf above [Le Brocq *et al.*, 2013]. This water acts to weaken the sediment, so allowing the fastest ice velocities above it [Siebert *et al.*, 2016]. For FIS, significant levels of water are provided by Academy Glacier (i.e. from East Antarctica), in which over a dozen 'active' subglacial lakes are known to exist all the way upstream to the Pole [Smith *et al.*, 2009; Jordan *et al.*, 2018]. Across the floor of the ice stream trunk, flow-parallel hard-rock landforms channel the water so that it too exits as a point source, leading to an ice shelf channel >130 km in length [Jeofry *et al.*, 2018b].

2.3 Sensitivity of the region to future change

The discovery that the IIS and MIS grounding lines are perched on the top of a major reverse bed slope revealed that they are potentially at a threshold of major glaciological change through marine ice sheet instability [Ross *et al.*, 2012]. This concern was added to by numerical ocean modelling, which predicted enhanced flow of warm water to the WS grounding lines by the end of this century as a consequence of wind-pattern changes offshore [Helmer *et al.*, 2012], suggesting the potential for future ice losses from this sector equivalent to ~0.3 m of sea level rise. To investigate the sensitivity of the WS sector ice streams to future ocean-driven warming, Wright *et al.* [2014] used the BISICLES ice sheet model (which includes appropriate grounding line physics) to determine grounding line dynamics of WS ice streams under ocean warming scenarios, leading to an appreciation of the conditions that deliver grounded ice retreat, and an understanding of the regions most sensitive to such change (Figure 2). The model was first run using best estimates of basal ice-sheet parameters, ice accumulation and grounding line melt rates. The first 'control' experiment ran this model for 2000 years, with the hope of replicating the present day ice sheet configuration. However, in this run, the IIS began to lose mass by around 200 years, and experienced accelerating mass loss in the subsequent 1800 years. By the end of the model run it was losing around 8 km³ of ice annually. Similarly, MIS lost mass at a rate of 1-2 km³ per year in the control experiment. This behaviour suggests that the two ice streams are not in equilibrium with the imposed forcing fields, so either these fields are wrong, or the ice streams are on the brink of major change. However, as Wright *et al.* [2014] state, the first

“run should therefore be viewed solely as a neutral starting point from which to assess the relative sensitivity of the ice streams to change, and not as a prediction”.

The model was then used in a series of experiments that adjusted the levels of ice accumulation and basal ice-shelf melting. Approximately ‘stable’ ice sheet configurations were obtained for runs where basal melting is reduced compared to the reference run, by as much as half the estimated values of today. However, when small increases were applied to the model, the IIS and MIS experienced mass loss and ice sheet retreat (Figure 2). Indeed, in all runs where increased melting was applied these two ice streams lost mass unabated throughout the 2000 years of the experiment. Other ice streams, such as Rutford Ice Stream and Carlson Inlet Glacier were relatively unaffected in the experiments, suggesting these ice flows are insensitive to small levels of increased rates of basal melting. However, when values around 25% more than today’s are used in the model, these glaciers also experience mass loss and ice retreat.

Clearly the model reveals that the IIS and MIS are the most sensitive in the WS to future ocean-driven change. Indeed the IIS appears to be the most sensitive of the entire WAIS in this regard [Cornford *et al.*, 2015]. Their retreat is halted when the entire Robin Subglacial Basin is deglaciated, and the bed slope returns to ‘normal’ (as opposed to reverse).

3. LGM ice-sheet configuration and LGM to mid-Holocene change

Hillenbrand *et al.* [2014] compiled ice core data (from Berkner Island and EPICA-Dronning Maud Land), marine geophysical measurements of former glacial landforms, marine sediment core information between the ice-shelf margin and the continental-shelf break, and onshore cosmogenic nuclide dating of rock exposures, to assemble two possible scenarios (A and B) describing the retreat of the WS sector between 20,000 years ago (i.e., the LGM) and 5000 years ago (the mid-Holocene). The two scenarios were based on different interpretations of dated material and on the style of glaciation.

Scenario MIN (Figure 3) is based largely on the onshore cosmogenic record [Bentley *et al.*, 2010; Le Brocq *et al.*, 2011; Whitehouse *et al.*, 2012a], and assumes that the oldest marine sediment dates represent minimum ages for post LGM ice sheet retreat. It also assumes that subglacial landforms on the present-day seafloor are pre-LGM in age. Scenario MIN also utilises an ice sheet model that matches where former ice surface elevation and extent have been constrained using dated onshore exposures. Scenario MAX (Figure 3) assumes that dates from sedimentary cores represent a mixture of maximum and minimum ages for the LGM and its retreat, and that the style of glaciation here was similar to that interpreted elsewhere in Antarctica at the LGM, where ice advanced to the continental shelf break. Scenario MAX requires that the vertical limits of fresh erratics around the WS embayment do not record the LGM limit [Bentley *et al.*, 2011; Clark *et al.*, 2011] and that the ice was substantially thicker without leaving a detectable geomorphological record. Importantly, both scenarios are consistent with low excess ice volumes during the LGM suggesting the region could only make a minor contribution to global meltwater pulses during the last deglaciation.

Scenario MIN at the LGM involves grounded ice extending across what is now the central FRIS to the continental shelf, with grounded-ice-free channels (e.g., Thiel Trough) to the east and west. At 15,000 years ago, Scenario MIN accommodates modest expansion of

grounded ice across the continental shelf, where ice-sheet extent is limited seaward of the KIR and HIR, and the Filchner/Thiel Trough is largely free of grounded ice (i.e. modest advance of the FIS). Grounded ice is predicted north of Berkner Island, but grounded ice is absent east and west of this advanced ice. By 10,000 years ago, grounded ice continuously covers the area between the present grounding line and the KIR and HIR. Grounded ice around Berkner Island is more extensive than today but is now cut off from the grounded WAIS. By 5000 years ago, the WAIS margin was similar to today, Berkner Island still contained more grounded ice than today and the KIR and HIR were joined but separated from the WAIS.

Scenario MAX starts with the grounded ice sheet fully expanded to the continental shelf, with continuous grounded ice across what is now the Ronne Filchner Ice Shelf. By 15,000 years, only modest retreat from this maximum position has occurred, and by 10,000 years continuous ice cover remains between Berkner Island, the Thiel Trough, and KIR/HIR. By 5000 years, the extent of grounded ice remains substantial; indeed greater in some places than the LGM configuration in Scenario MIN.

4. Radio echo-sounding and englacial structures

4.1 Background to radio-echo sounding

The two post-LGM scenarios discussed above are obviously in apparent conflict, although both feature a retreat from far out on the continental shelf at the LGM back towards the present-day configuration [Hillenbrand *et al.*, 2014]. Our review now concentrates on reconstructing the ice sheet history from the mid-Holocene (~5000 years ago), using a combination of glaciological data derived from glacier-geophysical investigations, with support from cosmogenic data in locations where both are in close proximity. The use of geophysical data from the ice sheet itself is possible and appropriate, as the ice itself is aged up to and older than 5000 years (accounting for accumulation, vertical deformation and lateral transport); hence changes to ice flow conditions around this time are recorded englacially. While we cannot comment on which of the two LGM scenarios are most accurate, we will comment on which of the two 5000 years reconstructions best fit with these observations.

The prime dataset used here is radio-echo sounding (RES), which can be mounted on aircraft or pulled by snowmobile. The RES technique operates through the emission of a radio wave which propagates through air and into the ice sheet, and is reflected off any boundaries separating media with differing dielectric properties [Siebert, 1999; Dowdeswell and Evans, 2004]. Radio wave reflections can be identified in RES data from the ice surface and the subglacial bed. In this way, information about Antarctic ice thickness, bed conditions and the distribution of subglacial water and lakes has been established [Dowdeswell and Evans, 2004]. In addition, Antarctic RES data show a number of strong reflections from within the ice sheet. The most widely noticeable of these englacial reflections are known as internal layers [Siebert *et al.*, 1999].

Because a radio wave reflection will occur at a boundary of dielectric contrast, the origin of internal layers must be a response to dielectric boundaries within the ice-sheet column. There are two possible causes of dielectric variation within the ice sheet: (1) ice density

and/or fabric changes, and (2) chemical properties of ice [see *Siegert et al.*, 1999]. Observations of density variation within ice cores indicate that density variation below about 500 m of ice depth will be too small to affect significant dielectric boundaries. Thus, an ice density origin for internal layering is only valid for the uppermost layers of the ice. However, variation in the chemistry of ice and crystal fabric can occur throughout the ice column. The most commonly held view is that dielectric variation is best explained by acidic layering within the ice sheet. Acidic layers originate from an aerosol product derived from volcanic eruptions that subsequently precipitates on the ice surface during snowfall. Burial of this snow eventually causes discrete layers of acid-laden ice at depth within the ice sheet. As ice flows within the ice sheet, these acid layers will deform accordingly. This deformation should result in folding of layers, but not necessarily cause discontinuities. Thus, internal RES layering below 500 m is expected to be continuous over several tens to hundreds of kilometres within central slow flowing regions of Antarctica [*Siegert*, 1999]. Such internal layers obey the law of superposition and represent isochronous surfaces.

However, where ice flows more quickly, internal layers buckle and become significantly disrupted and discontinuous. The transition between continuous and buckled layers mark shear zones of ice streams, or flow over major subglacial obstacles. If ice flow conditions have changed, the record of former ice flow is thus contained within englacial layers, but may be advected downstream or overprinted by subsequent accumulation. Hence, internal layer conditions are especially useful in determining ice-flow modifications in the last few thousand years.

Other englacial layers have been established close to the beds of ice sheets. Where englacial stress is enhanced as ice flows around large subglacial obstacles, crystal fabrics can develop, leading to permittivity layers. Fracture and crevassing of the ice at depth may also lead to distinctive changes in dielectric properties. In addition, layers resulting from accretion of ice from the bed, potentially also involving ice fabric development, have been seen in both slow [*Bell et al.*, 2011, *Wrona et al.*, 2018], enhanced [*Wolovick et al.*, 2016] and in transitional [*Bons et al.*, 2016; *Ross and Siegert*, 2014] regions of the ice sheet. In such cases, basal 'accretion' layers mark a transition between isochronous ice above (conformable with the basal layer, not necessarily the bed) and a basal ice unit with few noticeable layers or features.

Further englacial reflectors may result from basal sediment inclusion [*Siegert et al.*, 2013] and where ice is or has been floating, from basal crevasses [*Kingslake et al.*, 2018]. In all cases, interpreting past flow from internal layers requires consideration of how changes in time may affect layer arrangements. This becomes especially challenging where more than one type of change has occurred, leading to secondary episodes of deformation that may be challenging to distinguish. Nonetheless, analysis of internal layers and structures has proven very useful in determining the recent flow history of both the WAIS [*Siegert et al.*, 2004; *Catania*, 2012; *Conway*, 1999; *Martín et al.*, 2006; *Holschuh et al.*, 2018] and EAIS [*Bingham et al.*, 2007].

4.2 Glacial history of the SWSE sector from internal layering and basal features

We summarise englacial structures across the SWSE starting from the ice divide, across the transition to fast flowing ice and onto ice shelves and ice rises. The centre of the WAIS contains some of the clearest and best-preserved internal layers on the continent [Siegert and Payne, 2004]. Two sets of evidence support the idea that the ice-divide position is unlikely to have changed significantly between the LGM and today. First, by calculating former rates of ice accumulation necessary for the measured distribution of isochronous layers in a transect across the ice divide, it seems likely that the spatial pattern of accumulation has been unchanged in the last 20,000 years [Siegert and Payne, 2004]. If the ice divide had changed, the modification to the orographic influence on ice accumulation would lead to an accumulation distribution different in the past compared with today, as observed in Taylor [Morse *et al.*, 1999] and Talos [Siegert and Leysinger Vieli, 2007] ice domes. This is not observed across the WAIS, however, indicating ice divide stability. Second, small folds within internal layers, caused by ice flow across a rough bed from upstream, track downstream with ice flow. By tracing the troughs and peaks of internal layer folds, a pathway of former ice flow can be established, the date of which begins from when the furthest fold from the basal hill was positioned over it. Ross *et al.* [2011] calculate stability of the WAIS divide based on an assessment of internal layer structures over Lake Ellsworth experiencing no detectable change from the modern ice flow direction. A similar match between layer structures and modern ice flow is found on the WS side of the ice divide [Ross and Siegert, 2014] and in the Siple Coast [Holschuh *et al.*, 2018]. This is in contrast to the Siple Coast side, where ice flow direction has been shown to vary by around 30 degrees due to ice relaxation and retreat of grounded ice across the Ross Shelf since the LGM [Siegert *et al.*, 2004].

Further downstream, ice flows into the trunk of IIS through multiple subglacial valleys. Winter *et al.* [2015] analysed the internal layers within the Independence, Ellsworth and Horseshoe valley troughs, concluding that while the pattern of continuous versus disrupted layers is consistent with the modern flow of ice, supporting little ice flow direction change, evidence existed for former enhanced flow in these tributaries where ice is currently flowing slowly, suggesting ice dynamic change in the tributaries, if not in direction. Horseshoe Valley also contains basal ice structures associated with subglacial hills and pinnacles that are best explained as inclusions of basal sediment [Siegert *et al.*, 2013]. The feature can be tracked downstream to the trunk of IIS, but no internal layers exist within it preventing further tracking (Figure 4).

The next location to consider is the BIR, adjacent to the IIS and MIS, which contains key glaciological data constraining the Holocene glacial history of the SWSE. Presently the BIR contains only very slow flowing ice. Most stable ice rises that are frozen at their beds have well-established 'Raymond arches' beneath their ice divides, which form as a consequence of non-linear variation in ice rheology with strain rate and stable flow over one characteristic time; the time taken to accumulate the full ice thickness [Raymond, 1983; Martín *et al.*, 2009]. Ice rises that do not contain Raymond arches are either too young, or have experienced ice divide migration. The BIR contains a small Raymond arch beneath its divide, suggesting recent stability, but not long enough for a major arch to develop [Martín *et al.*, 2009]. Satellite imagery reveals the BIR to have relic flow stripes across its surface (Figure 5, 6), indicating the direction of former ice flow was similar to the present flowpath of ice within the adjacent Moller Ice Stream (MIS) [Siegert *et al.*, 2013]. Beneath the surface, radar has measured buckled internal layers under continuous layers, indicative of ice-

dynamic processes being suddenly replaced by stagnant flow (Figure 6). One conclusion to be drawn from these two datasets is that the past ice flow direction across the BIR was aligned with the surface stripes at enhanced flow speeds. Flow would have tracked across what is now the trunk of IIS, emanating from the three tributaries the other side of it (i.e. Ellsworth, Independence and Horseshoe valleys). *Siegert et al.* [2013] used a simple 1-dimensional ice compression model, and the modern rate of ice accumulation, to estimate the age of the transition between continuous and buckled layers at around 5000 years ago.

The radar data also show the bed of BIR to be extremely smooth and continuous between it and the IIS trunk. Hence, the shear margin between the IIS and BIR should be controlled by basal hydrology and thermo-mechanics; on one side the IIS is wet based and on the other the BIR is cold based (Figure 6). The shear margin between BIR and MIS is tectonically influenced by the Pagano Shear Zone [*Jordan et al.*, 2013], and may represent a more stable border between fast and slow flow. In summary, these data show that the IIS used to once track across the BIR, and over what is now its hydrologically-controlled shear margin.

Another interesting englacial feature across BIR is an apparent basal layer [*Siegert et al.*, 2013] (Figure 6), which looks remarkably similar in appearance to the sediment inclusion observed in Horseshoe Valley. It can be traced across the entire BIR along a former flowband (i.e., flow stripes). Interpolation upstream (across what is now the IIS trunk) links it to the feature in Horseshoe Valley, though without drilling through the ice and sampling it is not possible to be certain whether this is the same feature. An alternative explanation for the BIR basal feature is that it represents crevasses along a former shear margin, that have been subsequently filled with salt-water.

To the north of BIR, adjacent to the ice plain that separates the grounded ice from the ice shelf, englacial folds can be observed, which are consistent with recent localised advance (i.e. 10-20 km) of the grounding line and expansion of the ice rise. Further downstream, embedded within the Ronne Ice Shelf, are the KIR and HIR, and the Doake Ice Rumples (Figure 7). Ice rises are independent flow features with ice flow emanating from their center to the grounding line surrounding them. In contrast, at ice rumples an ice shelf becomes temporarily grounded and slows significantly before becoming afloat at their downstream grounding line. The flow of the ice shelf is heavily modified by the presence of the relatively slow-flowing ice rises and rumples. HIR is approximately 100 km north-east of BIR. Ice from the MIS flows past its eastern flank, ice from IIS flows past HIR to the west over Doake Ice Rumples, and ice flowing off the front of BIR flows very slowly towards HIR before being diverted westwards at HIR's southern flank. KIR lies approximately 200 km to the west of HIR, with ice from IIS flowing past both flanks.

In terms of glaciological setting and planform size, HIR and KIR are similar. Ground-based, 4 MHz RES surveys conducted in 2013/14 and 2014/15 revealed that they differ significantly in thickness and in englacial structure. KIR consists of a single ice divide, approximately 150 km long, running approximately SW-NE. KIR is approximately 600 m thick at its summit. The bed of KIR is flat and smooth and englacial layers are smooth and conformable everywhere that we have RES data. Beneath the ice divide are prominent Raymond Arches running the length of the ice divide [see *Kingslake et al.*, 2016].

HIR consists of two ridges, each approximately 100 km long, extending to the north and south-west from a peak in surface elevation in the south-east. In contrast to the surface

topography, a basal high point is located at the northern end of the northern ridge [Kingslake *et al.*, 2018]. HIR is 400 - 800 m thick. There are only small, under-developed Raymond Arches in HIR, and these are restricted to the northern end of the northern ridge. Elsewhere, Raymond Arches are undetectable. This suggests ice flow has not been stable here for the characteristic time [Martín *et al.*, 2009] of approximately 4.5 kyr (estimated from the radar-derived measured ice thickness and a range of accumulation rates from satellite data [Arthern *et al.*, 2006] and modelling [van Wessem *et al.*, 2018]. From the ground-based ice-penetrating radar survey, continuous regions of bright tilted reflectors are observed at the base of HIR up to 12 km inland from the grounding line of the northward pointing promontory (Figure 7). These reflectors are distinct from the ubiquitous internal layers also observed in HIR. Individual dipping reflectors extend vertically 150-200 m into the ice from the base and span up to 2 km horizontally. The isochronal layers intersected by the dipping reflectors decrease in age as one moves toward the grounding line. This is consistent with these reflectors being relic basal crevasses, formed in a previous flow configuration, when the grounding line was upstream of its present location. Basal crevasses likely formed as vertical features at former grounding lines and filled with seawater which froze, leading to the high dielectric contrast that generates the reflection in radar data. The ice-rise grounding line advanced through this region and once grounded basal crevasses were deformed by vertical shear leading to their tilt.

Also found within these regions of bright reflectors are troughs in internal layering. They are continuous across radar lines. It is thought that these features form as a result of concentrated basal melting at former grounding lines, as observed at former shear margins on the Siple Coast [Catania, 2006]. The spatial distribution of relic basal crevasses and melt synclines (Figure 7), suggests ungrounding of the northern basal high, as part of a complete or only partial ungrounding of HIR. We expect ice rises to remain grounded over their high points if they form during a period of ice sheet retreat [Favier and Pattyn, 2015], so these observations indicate complete ungrounding, but we cannot rule out partial ungrounding.

The advance of the grounding line surrounding HIR towards its present-day position is estimated to be 6 ± 2 kyr. Their model simulates the vertical deformation of basal crevasses from their height at formation to the height as observed with RES, while accounting for uncertainty in accumulation, firn density, RES-derived depth, ice-thickening history, initial crevasse height and Glacial Isostatic Adjustment (GIA).

Overall, ground-based RES surveys of HIR and KIR have highlighted stark differences in their internal structure that has been interpreted to be reflective of the two features having contrasting recent flow histories.

5. Cosmogenic nuclide evidence of ice sheet reconfiguration

5.1 Cosmogenic nuclide methods

In situ cosmogenic nuclide dating of formerly exposed rock and sediment is the only feasible method to date the timing and trajectory of past ice thickness changes in Antarctica. *In situ* cosmogenic nuclides are formed in material at the Earth's surface through interaction with secondary cosmic radiation. The flux of cosmic radiation decreases exponentially in the subsurface as particles interact with the solid earth. Many cosmogenic nuclides are

produced through this interaction, and their concentration in surface rocks can be used as a chronometer indicating the duration of time spent at or within the upper few meters of Earth's surface [LaI, 1991]. The method is widely used to reconstruct ice histories because glaciers are highly erosive and generally effective at eroding their beds deeper than a few meters. Therefore, erratics, moraine boulders or the ice-moulded bedrock left behind as the glacier recedes are usually "fresh", with the cosmogenic nuclide inventory having been fully reset. In this way, given knowledge of production rates, the measured concentration of cosmogenic nuclides that have built up subsequently in the dated surface can be used to determine an apparent "exposure age" for that surface. The apparent exposure age may closely date ice retreat or thinning from that position providing the surface has subsequently remained continuously exposed with minimal rock surface erosion. The exposure dating method has been used extensively in Antarctica to constrain past ice sheet elevation change by dating erratics deposited on the flanks of nunataks as the ice sheet thinned. In this way, the nunataks act as dipsticks that record the changing elevation of the ice sheet through time, and the approach has proved highly effective at many locations in Antarctica [Hein et al., 2016b; Jones et al., 2015, Balco, 2011; Mackintosh et al., 2007; Stone et al., 2003].

Exposure dating in Antarctica is sometimes complicated by ineffective erosion beneath, and burial by, non-erosive ice. In this case, the cosmogenic nuclide inventory is not fully reset between periods of glacial cover. Where erratics and sediment have been buried by cold-based ice, the assumption of continuous exposure since deposition is violated, and exposure dates from these surfaces will not date the last thinning of the ice sheet. These and other processes can introduce geological scatter into cosmogenic nuclide datasets, which complicates the interpretation of exposure ages in terms of ice-sheet thinning. Measurement of multiple cosmogenic nuclides with different half-lives can be used to assess whether a rock surface has experienced a simple exposure history involving continuous surface exposure, or a complex exposure history involving periods of burial under ice. In the latter case, the shorter-lived isotope will preferentially decay when buried by ice, causing a detectable change in the isotopic ratio [LaI, 1991]. Most studies to date have used the cosmogenic $^{26}\text{Al}/^{10}\text{Be}$ pairing, since both isotopes are produced in quartz and are easily measured in the same rock. However, the half-life of ^{26}Al (0.705 Ma) is just half that of ^{10}Be (1.389 Ma), so only very long periods of burial on the order of hundreds of thousands of years can be detected using this method. More recently, measurement of *in situ* ^{14}C in quartz has become possible, and its short half-life (5,730 a) makes it highly sensitive to exposure and burial over the past ~25 ka. For example, ^{14}C paired with a longer-lived isotope such as ^{10}Be , can detect burial periods as short as a few thousand years, making it highly useful for unravelling ice sheet change over the Late-glacial to Holocene period [Goehring et al., 2011; Goehring et al., 2019; White et al., 2011].

Most cosmogenic nuclide studies to date have focussed on measuring cosmogenic ^{10}Be in subglacially derived, sometimes striated cobbles deposited on bedrock on the flanks of Antarctic nunataks. The cobbles are preferred because they often retain a sub-angular to sub-rounded shape that is typical of subglacial sediment transported by erosive, warm-based ice. These erosive conditions should produce "fresh" surfaces with minimal nuclide inheritance. The preservation of striations also indicates minimal erosion of the rock surface after deposition. Exposure dates from locations where these sample characteristics are common can produce clear thinning histories with little geological scatter in exposure age results [e.g., Hein et al., 2016b; Jones et al., 2015]. In other settings, the success of the

method is highly variable. For example, in the Pensacola Mountains, *Balco et al.* [2016] and *Bentley et al.* [2017] independently sampled altitude profiles in the Williams Hills that indicated at least 450 m of thinning occurred from the LGM through the Holocene, while a similar altitude profile from the Schmidt Hills, just tens of kilometres downstream, yielded ^{10}Be exposure ages that predate the last glacial cycle, and imply no thinning at all, which is hard to reconcile with the data from Williams Hills. The contrast is likely to do with specific flowlines of ice streams and tributary glaciers, as well as transitions between warm- and cold-based ice [*Bentley et al.*, 2017]. It is situations like these where the measurement of *in situ* ^{14}C can be advantageous [e.g., *Balco et al.*, 2016]. Recent analysis of *in situ* ^{14}C from the Schmidt Hills indicates at least 800 m of thinning occurred after the LGM [Nichols et al., 2019]. Likewise, *in situ* ^{14}C analysis of rocks from the Shackleton Range indicate the Slessor Glacier thinned by at least 300m and, perhaps as much as 650 m, following the LGM; this result contrasts with long-lived isotopes that imply no thinning at all, and demonstrates the utility of *in situ* ^{14}C at sites where nuclide inheritance is problematic [Hein et al., 2011; 2014; Nichols et al., 2019].

5.2 Data from the SWSE sector and surroundings

Changes in the Holocene elevation of the ice-sheet surface in the heart of the SWSE have been studied in the southernmost Ellsworth Mountains, notably the Patriot Hills, Marble Hills and Independence Hills [*Bentley et al.*, 2010; *Hein et al.*, 2016a; *Hein et al.*, 2016b; *Johnson et al.*, 2019]. It has also been used on material from the Pensacola Mountains, where cosmogenic exposure data show the thinning history at Mt Bragg and Mt Harper, recording past elevation change of the Academy Glacier, and the Williams Hills and Thomas Hills adjacent to the FIS [*Balco et al.*, 2016; *Bentley et al.*, 2017]. In all areas the pattern is similar but with minor differences in timing, namely that the altitude profiles show ice sheet thinning that reached the level of the present day ice in the Late Holocene (Figure 8). The data are consistent with the two Holocene ice history scenarios noted previously, but currently cannot distinguish between them. The first scenario is that the ice reached present day ice level in the Late Holocene and thinned no further, staying at the same level since that time to present (Scenario A in Figure 5). A second scenario is where the ice thinned below the present-day level in the Late Holocene and only subsequently thickened to present levels (Scenario B in Figure 5).

In the Ellsworth Mountains, the more recent work relies on cosmogenic nuclide $^{26}\text{Al}/^{10}\text{Be}$ pairing on quartz and ^{36}Cl from limestone samples of unweathered and often striated glacial erratics [*Hein et al.*, 2016]. Field observations and airborne radar shows that these erratics have been derived from the glacier base and been brought to the ice surface in a blue-ice ablation area. On the mountain slopes above the present ice surface such erratics have been deposited as a veneer of perched blocks. The upper limit of such fresh erratics demonstrates the maximum thickness of the Weddell Sea sector of the ice sheet during the LGM; a state that persisted until the beginning of the Holocene. Cosmogenic exposure-age transects from the upper limit to the present ice record the history of thinning of the ice during the Holocene at a location close to the present grounding line in Hercules Inlet.

The upper limit of unweathered erratics shows that the ice was up to ~475 m thicker than present in the southernmost Ellsworth Mountains during the LGM [*Hein et al.*, 2016b;

Bentley et al., 2010]. The range of dates at the upper limit of 49-10 ka encompasses the peak of the LGM at ~21 ka, and could imply that thick ice persisted throughout the warming of the late-glacial (~18-10 ka). It seems reasonable to argue that this persistence reflects the increased snowfall and ice accumulation associated with warming as shown in the WAIS ice core [WAIS Drilling Project, 2013]. Importantly, the direction of flow of the thicker ice sheet was eastwards towards BIR [cf. Siegert et al., 2013]. This is shown by erosional landforms, erratic trains of known lithology and the orientation of a blue-ice moraine immediately north of Independence Hills.

The vertical transects, taken together, show that the ice sheet surface in the Ellsworth Mountains began to fall about 10 ka and had reached the present level by 3.5 ka. Moreover, there was a pulse of rapid thinning of ~400 m at 6.5-3.5 ka that, if extrapolated around the Weddell Sea Embayment, would have contributed 1.4-2 m to global sea-level rise [Hein et al., 2016b]. What is interesting is that the geomorphology, changes in direction of ice flow of glaciers into Horseshoe Valley, and the disruption of blue-ice moraines linked to the eastward flow of thicker ice, accompanied or followed this sharp pulse of thinning. The most likely reason is that the migration of the grounding line into the troughs of IIS and Hercules Inlet captured the eastward ice flow towards BIR from the Horseshoe Valley.

In the Pensacola Mountains the ice sheet history is consistent with that for the southern Ellsworth Mountains. The Academy Glacier thinned similarly rapidly through the Holocene and reached present levels by 2.5 ka, whilst a few 10s of kilometres away, the FIS had thinned at least a few 100m to within 40m of present levels in the Williams Hills by 5.2 ka [Bentley et al., 2017; Balco et al., 2016; Nichols et al., 2019]. A mid-Holocene pulse of thinning of similar scale and magnitude has also been reported from the Lassiter Coast in the western WSE based on *in situ* ¹⁴C ages [Johnson et al., 2019]. Here, the ice elevation fell from 385 m to 138 m above modern ice between 6.0 ± 0.5 to 7.5 ± 0.7 ka.

6. Solid Earth measurements and modelling

6.1 Ice dynamics, solid Earth deformation, and sea-level change

The evidence reviewed above does not allow us to distinguish between the two scenarios proposed for the recent glacial history of the SWSE. Therefore, in an attempt to fill some of the spatial and temporal gaps in the data, we turn to the insight that can be provided by ice-sheet and solid-Earth modelling. Numerical ice-sheet models, driven by changes in climate, can be used to predict changes in ice flow and thickness which can be compared with evidence from RES and cosmogenic exposure dating. The solid Earth and sea-level response to these changes in ice loading can be predicted using a GIA model, and compared with GPS-derived estimates of present-day surface deformation and geological evidence for relative sea-level change.

Feedbacks between the ice sheet, the solid Earth and sea-level change likely played an important part in controlling the behaviour of the SWSE during the late Holocene. Such feedbacks have the potential to stabilise [Gomez et al., 2010] or destabilise [Siegert, 2001] the ice sheet, and both types of behaviour have been reproduced by numerical models. Studying the strength of the various feedbacks, either via modelling of model-data

comparisons, helps us to determine which processes ultimately governed the evolution of the WS sector during the late Holocene.

Marine ice sheet instability (MISI) describes the process whereby grounding line retreat on a reverse-bed slope leads to an increase in ice thickness at the grounding line (because the bed deepens upstream), and hence an increase in ice flux across the grounding line [e.g., *Joughin et al.*, 2014]. If this increase in flux is not balanced by an increase in accumulation this can lead to runaway retreat until the bed begins to shallow, and ice thickness reduces, again upstream. Along many of the ice streams in the SWSE the bed deepens inland so, if the MISI was the dominant process controlling ice sheet dynamics, we might expect the grounding line to have retreated continuously from an LGM position somewhere on the continental shelf to a stable position upstream of the present grounding line. Instead, the present-day grounding line is perched part-way along the reverse-bed slope that extends from the continental shelf to regions such as the Robin Subglacial Basin [*Ross et al.*, 2012]. The reason for the apparently unstable position of the present-day grounding line is likely linked to the presence of the Ronne Filchner Ice Shelf, which exerts a significant buttressing effect on the grounded portion of the ice sheet and the presence of large ice rises (*Matsuoka et al.*, 2015). Indeed, *Whitehouse et al.* [2017] used a numerical flowline model to demonstrate that ice shelf collapse would lead to grounding line retreat behind present, but that ice shelf re-growth would rapidly allow the grounding line to readvance to its observed position along the FIS (Figure 9).

In addition to the buttressing provided by the Ronne Filchner Ice Shelf and its ice rises, isostatic uplift in response to ice loss may also have helped to stabilise the WS sector of the ice sheet during the late Holocene. As an ice sheet thins or retreats the net reduction in surface loading, after accounting for the flux of ocean water into the space left by a retreating ice sheet, triggers viscoelastic rebound. The wavelength of the rebound will depend on the thickness of the lithosphere, while the magnitude and time dependence will be controlled by the viscosity structure of the mantle [*Nield et al.*, 2018]. In tandem with the uplift of the bed, the decreasing mass of the ice sheet leads to a decrease in the gravitational attraction exerted by the ice sheet on the ocean, and hence a drop in the local height of the geoid, i.e. the sea surface [*Gomez et al.*, 2010]. The net effect of these two GIA-related processes is a decrease in the water depth at the grounding line, which, if large enough, has been hypothesized to have the potential to slow, or even reverse, unstable grounding line retreat [*Gomez et al.*, 2015; *Konrad et al.*, 2015; *Kingslake et al.*, 2018]. In addition to reducing water depth at the grounding line, the reduction in water depth offshore can help to promote ice rise formation, thus increasing the buttressing effect of the ice shelf [*Favier and Pattyn*, 2015].

The spatio-temporal history of isostatic rebound during the late Holocene, and the degree to which it has played a role in governing the evolution of the SWSE, is poorly known. The spatial pattern of rebound will depend on the history of both ice thickness change and grounding line retreat across the Weddell Sea embayment; a region that is currently covered by the FRIS. Ice sheet modelling provides some insight into possible configurations of past retreat [e.g., *Golledge et al.*, 2014; *Maris et al.*, 2014; *Pollard et al.*, 2017], with large-scale constraints on past ice thickness and grounding line extent available from ice cores recovered from ice rises [e.g., *Mulvaney et al.*, 2002].

The second factor that controls the rate of isostatic rebound is the rheology of the solid Earth. Mantle viscosity is hypothesized to be relatively high across the southern part of the SWSE [$\sim 10^{21}$ Pa s, *Whitehouse et al.*, 2019], but there is limited information on the rheology beneath the outer part of the embayment due to poor coverage by seismic stations [*Shen et al.*, 2018]. High mantle viscosity can be related to a long decay time [*McConnell*, 1965], and hence rebound in response to post-LGM ice loss is likely to be ongoing today across the southern portion of the SWSE, with the caveat that the timing of post-LGM ice loss is poorly known. When seeking to reconstruct past ice sheet change using contemporary rates of solid Earth deformation, the trade-off with Earth rheology leads to significant non-uniqueness [*Whitehouse*, 2018], with an additional complication being that the loss of ice close to flotation will trigger a limited isostatic response. Feedbacks between ice dynamics and isostatic rebound will be greatest in regions where there has been a significant decrease in the thickness of ice above flotation.

In summary, isostatic rebound may have reduced the rate of grounding line retreat, promoted the likelihood of ice rise formation, or even triggered grounding line re-advance across the SWSE and wider WS sector during the late Holocene. If re-advance did take place, and was accompanied by sufficient ice thickening above flotation, this will have damped the rebound process, and contemporary uplift rates would be smaller than expected in a scenario of monotonic ice loss and retreat. The following two sections briefly outline what is known about isostatic rebound across the WS sector, and how these observations compare with recent modelling efforts.

6.2. Data from the SWSE and surrounding

Records of isostatic rebound across the SWSE are limited to a small number of GPS sites that record contemporary solid Earth deformation. The traditional approach of reconstructing millennial-scale solid Earth deformation via the interpretation of relative sea-level records is not possible due to the complete lack of exposed coastline in the region. In other regions, relative sea-level records have traditionally been used to determine the relaxation time, and hence the viscosity, of the mantle [e.g. *Mitrovica and Forte*, 2004]. The short time span of the GPS data in the SWSE provides no insight into the relaxation time of the mantle, and this exacerbates the issue of non-uniqueness when seeking to use the GPS rates to infer the history of past ice sheet change.

The sparse spatial coverage of bedrock GPS sites is related to the lack of outcrops in the region; currently, no techniques exist for measuring isostatic rebound beneath regions of grounded or floating ice. It is logistically challenging to regularly access the bedrock GPS sites to download data and service the instruments. This is changing as the majority of instruments now have the capacity to transmit data and state-of-health information in real time, but there are significant historical data gaps in many records, and these are reflected in the large uncertainties associated with deformation rates at many sites. Published GPS rates across the region span -2.20 to +7.04 mm/yr, but typically have uncertainties on the order of 1-2.5 mm/yr [*Wolstencroft et al.*, 2015; *Bradley et al.*, 2015]. Extending the temporal and spatial coverage of measurements that reflect the contemporary pattern of solid Earth deformation across the WS sector would provide invaluable insight into recent ice sheet change and the stability of the current ice sheet configuration. Spatially-continuous estimates

of isostatic rebound are beginning to be derived via data inversion, whereby satellite gravimetry and altimetry data are combined to simultaneously invert for contemporary ice mass loss and the GIA signal, often also incorporating GPS observations [Gunter *et al.*, 2014; Martín-Español *et al.*, 2016a; Sasgen *et al.*, 2017; Engels *et al.*, 2018]. Uncertainties are large, due to assumptions related to the interpretation of satellite data, but at least they can be formally quantified in this independent, data-driven approach.

6.3 Modelling and plausible ice sheet reconstructions

GIA modelling can be used to predict the pattern and magnitude of isostatic deformation across the WS sector for the post-LGM period. A ‘forward’ GIA model requires inputs of ice history and Earth rheology, and this permits the calculation of spatially-varying sea-level change and solid Earth deformation [e.g. Whitehouse *et al.*, 2012b; Ivins *et al.*, 2013; Argus *et al.*, 2014; Briggs *et al.*, 2014]. To better understand the impact of isostatic rebound on ice dynamics, GIA model output relating to the uplift history of the WS sector could be prescribed as an a priori boundary condition for ice sheet modelling. However, there is currently considerable uncertainty regarding the pattern of GIA-related solid Earth deformation across the wider WS sector.

GIA model predictions of present-day uplift rates across the WS sector vary significantly in both spatial pattern and magnitude [Whitehouse *et al.*, 2019]. The majority of models predict maximum present-day uplift rates in the region of the HIR, KIR and BIR, with predicted rates peaking at >10 mm/yr [Whitehouse *et al.*, 2012b; Argus *et al.*, 2014]. Models that incorporate 3D variations in mantle rheology may predict both faster [A *et al.*, 2013] and slower [van der Wal *et al.*, 2015] uplift rates compared with calculations that combine the same ice history with a simple 1D profile of mantle viscosity. The predictions of Ivins *et al.* [2013] have a very different spatial pattern, with maximum uplift rates of only ~5 mm/yr predicted for the south-west Weddell Sea region and negligible (<2 mm/yr) rates predicted for the central southern Weddell Sea embayment. The history of post-LGM deformation will also vary considerably between models. These differences between GIA model predictions arise primarily due to a lack of constraints on post-LGM ice sheet configuration, which has led to there being significant differences between the ice history models adopted in the different GIA models. None of the models provides a good fit to the regional uplift pattern documented by GPS [Martín-Español *et al.*, 2016b].

Most Antarctic GIA modelling studies are motivated by the desire to test a new data- or modelling-constrained reconstruction of past ice sheet change within a GIA framework [e.g., Whitehouse *et al.*, 2012a, b]. In contrast, Bradley *et al.* [2015] sought to explain the surprising observation that a GPS site in the Ellsworth Mountains, a region expected to be uplifting in response to post-LGM ice mass loss, was subsiding. They calculated the isostatic response to a suite of hypothesized ice history scenarios, including an approximation of the two scenarios proposed by Siegert *et al.* [2013], and found that the GPS observations could not be explained by monotonic post-LGM ice loss, i.e. scenario A. Instead, the data required there to have been a period of either ice thickening or re-advance during the late Holocene [Bradley *et al.*, 2015]. The study was unable to provide detailed insight into the position of the grounding line during the late Holocene, primarily due to the fact that any advance or retreat of grounded ice close to flotation would have left a negligible isostatic fingerprint.

There is clearly a significant range in model predictions of isostatic rebound across the WS sector leading to uncertainty in efforts to quantify the impact of this rebound on ice sheet dynamics during the late Holocene. Many ice sheet models include an isostatic component [e.g., *Bueler et al.*, 2007], but they are unable to account for the second feedback associated with GIA, which is the local drop in the height of the sea surface associated with a decrease in the mass of the ice sheet. This can only be determined by running a GIA model that accounts for the global redistribution of meltwater across the ocean. The most self-consistent approach to determining feedbacks between GIA and ice dynamics is therefore to run a coupled model [e.g., *Gomez et al.*, 2013; *de Boer et al.*, 2017]. However, a significant limitation of this approach, aside from the uncertainty associated with climate forcing, is the need to know the correct Earth rheology. Upper mantle viscosity across Antarctica is thought to vary by >3 orders of magnitude [*van der Wal*, 2015; *Hay et al.*, 2017; *Whitehouse et al.*, 2019]. The associated range in mantle relaxation times significantly perturbs the strength of the feedback between isostatic deformation and ice dynamics in different regions of Antarctica [*Gomez et al.*, 2015; *Konrad et al.*, 2015; *Pollard et al.*, 2017] and motivates the need for a coupled ice sheet-GIA model that incorporates 3D Earth structure. *Gomez et al.* [2018] use such a model to quantify the effect of incorporating 3D variations in mantle viscosity compared with a more common 1D radial profile of mantle viscosity. Differences in predicted ice thickness in the southern Weddell Sea region are on the order of several hundred metres during the Holocene, with implications for grounding line position. Similarly, they predict differences in relative sea level and contemporary uplift rates between the 1D and 3D models on the order of tens of metres during deglaciation, and several mm/yr at the present day, respectively. Such models are rapidly enhancing our ability to explore the drivers of ice sheet change in the WS sector, but a crucial outstanding issue is the need to simultaneously represent feedbacks between ocean forcing and ice shelf evolution [*Asay-Davis et al.*, 2016]. The buttressing provided by ice shelves plays a significant role in controlling the stability of the ice sheet [*Wright et al.*, 2014], and ice shelf thickness directly determines whether ice rises are able to form as a result of isostatic rebound.

We close this section by reviewing the results of ice-sheet modelling studies that are not coupled to a GIA model, but that do incorporate some component of solid Earth rebound. It is interesting to note that model-derived ice sheet reconstructions predict grounding line retreat behind present, and subsequent readvance, at some point during the Holocene, at a range of locations around the southern Weddell Sea [*Golledge et al.*, 2014; *Maris et al.*, 2014; *Pollard et al.*, 2017; *Kingslake et al.*, 2018]. These studies use different numerical ice sheet models, and they differ in their approach to climate forcing, ice sheet basal conditions, and ice shelf dynamics, but all represent an attempt to reconstruct the history of the WAIS since the LGM. This is not to say that all modelling attempts reproduce grounding line retreat behind present; the ensemble analysis of *Briggs et al.* [2014] does not appear to predict Late Holocene readvance in the wider WS sector, while in the studies of *Pollard et al.* [2017] and *Kingslake et al.* [2018] model scenarios that involve faster rates of rebound predict slower rates of ice loss and no retreat behind present. This is due to the damping effect of the rapid rebound.

In this section we have summarised the ice sheet and solid Earth modelling efforts that provide insight into the processes controlling recent ice sheet change in the SWSE and wider WS sector. As may be expected, standalone and coupled ice sheet models are able to reproduce a range of scenarios that encompass the retreat histories suggested by the

glaciological and geological data documented above. However, it appears that the rate of isostatic rebound potentially plays a crucial role in determining the details of the retreat. On one hand, isostatic rebound can act to slow the rate of grounding line retreat, which would be compatible with the hypothesis that the grounding line is currently in its most retreated position since the LGM (Scenario A). Alternatively, isostatic rebound may have helped trigger ice rise formation and grounding line readvance subsequent to retreat behind present at some point earlier in the Holocene (Scenario B). Ultimately, additional data are needed to resolve the details of recent ice sheet change, and provide further insight into the strength of the feedbacks operating between the ice sheet, the solid Earth, and the ocean.

7. Holocene glacial history

7.1 Ice flow at and before mid-Holocene

Geophysical data from the ice sheet and exposed rocks point consistently to major ice sheet change in the WS sector at around 5000 years. Buckled layering in the BIR, beneath continuous layers dated to around 5000 years, coupled with palaeo flow stripes across the ice rise, are clear indicators that the ice location was once covered by fast flowing ice. The flow stripes point to an origin from the IIS tributaries, parallel to the modern flow of MIS. This is also consistent with basal features that can tentatively be correlated between BIR and Horseshoe Valley. We are unable to explain whether the ice across BIR was floating (i.e., a fast flowing section of an ice shelf emanating from upstream IIS) or a ice stream grounded across the Robin Subglacial Basin and BIR, however.

Beneath the ice divide on KIR a prominent Raymond Arch suggests stable flow here during at least the past 2-3 kyr [Kingslake *et al.*, 2016]. Further north along the KIR divide, polarimetric phase-sensitive radar and active seismic surveys reveal a transition in englacial fabric at around 200-230 m depth [Brisbourne *et al.*, 2019]. These authors interpret the fabric beneath this depth as evidence of a change in past flow conditions. Specifically, the observations can be explained by previous flow aligned approximately along the ice divide, away from IIS. Tracing stratigraphy back to the divide used to date the formation of Raymond arches [Kingslake *et al.*, 2016], indicates that the change from this previous SW-NE flow regime occurred around the time of Raymond Arch formation (2-3 kyr). There is no englacial stratigraphic evidence for past fast flow at KIR, and because 2-3 kyr is not long enough for such evidence to flow out of KIR, we can conclude that at least immediately prior to the onset of ice divide flow (and the formation of the Raymond arches), flow was not fast over KIR. This does not rule out a previous period of fast flow over KIR and even regrounding of the ice shelf in this location if it occurred long enough in the past for any englacial evidence of fast flow, as is seen in BIR and HIR, to advect out of the region surveyed by Kingslake *et al.* [2016].

The lack of mature Raymond Arches on HIR suggest that ice flow has not been stable here for at least the characteristic time of the ice rise [Martin *et al.*, 2009], approximately 4.5 kyr. The complex englacial structure of HIR can be explained if the grounded area of the ice rise was smaller in the past and readvanced towards its current position at around 6 kyr. Without a previously smaller ice rise and a subsequent advance of the grounding line to its present

location, it is difficult to explain the spatial pattern of the interception between isochrones and steeply-dipping englacial layers interpreted as marine-ice-filled relic basal fractures.

Two interpretations are possible as to the minimum extent of HIR during the Holocene. In one interpretation the ice rise ungrounded completely; this can explain all the unusual englacial structures observed. Alternatively, the ice rise ungrounded from the northern subglacial topographic high, but remained grounded over deeper regions. Based on our limited understanding of ice rise formation and subsequent evolution, this appears unlikely; it is inconsistent with recent idealized modelling of ice-rise dynamics [Favier *et al.*, 2015]. While a smaller-than present HIR that nonetheless persisted throughout the Holocene cannot be ruled out, until a deeper understanding of ice-rise flow dynamics and independent constraints on the spatial extent of the ice rise are obtained, the interpretation that the ice rise ungrounded completely during initial post-LGM ice sheet retreat and later regrounded, perhaps due to GIA (section 6) is consistent with this argument.

Some modelling studies pertain to the question of whether ice rises in the Weddell Sea ungrounded during the Holocene (Section 6.3). For example, Kingslake *et al.* (2018) examined the hypothesis of a complete Holocene ungrounding of HIR and its implications using an ice-sheet model that incorporates simplified GIA physics. They were able to reproduce the situation where all three ice rises ungrounded after the LGM. Despite limitations related to resolution and bed topography, this suggests ungrounding was possible, but depends sensitively on, among other factors, the solid Earth and ice properties prescribed in the model, the climate, and the LGM extent of the ice sheet.

7.2. Ice relaxation model: mid-Holocene to today

In this model, gradual retreat of the grounding line to the position at 5000 years, with associated ice thickness reduction and crustal uplift, led to relatively high ground beneath the ice rises. This caused rerouting of water from the palaeo IIS trunk into the Robin Subglacial Basin, and both slow cold-based flow over the BIR and the creation of today's fast flowing IIS along the subglacial basin. Evidence in support of this idea comes from the shear margin between IIS and BIR, which is a hydrological one, and from the Siple Coast, where subglacial water migration is thought to be key in the shutting down and activation of ice streams [Anandakrishnan and Alley, 1997]. It is possible that either Scenario MAX or Scenario MIN of Hillenbrand *et al.* [2014] at 5000 years is consistent with this model. (Figure 3).

7.3 Ice sheet retreat and readvance model: mid-Holocene to today

An alternative explanation is that the ice margin retreated upstream of today's position, deglaciating the Robin Subglacial Basin. During this time an ice shelf persisted across the current location of the BIR/KIR/HIR, and it became grounded sometime during the mid-to-late Holocene due to post-LGM isostatic uplift. This grounding led to the build-up of the ice rises, blocking fast-flowing ice, and leading to the re-routing of the IIS to the west of BIR, and MIS to its east. Evidence in support of this includes the englacial stratigraphy discovered within HIR and the buckled internal layers at the northern edge of BIR. In addition, the low

GPS uplift rates recorded in the Ellsworth Mountains have been interpreted to reflect the damping effect of ice sheet readvance on post-LGM rebound [Bradley *et al.*, 2015]. Models that incorporate both ice sheet dynamics and glacial rebound reveal how this scenario is possible [e.g. Kingslake *et al.*, 2018] but the details depend on poorly quantified factors such as Earth rheology, seafloor topography, and ocean-ice shelf interactions.

7.4 Cosmogenic nuclide evidence: mid-Holocene to today

Cosmogenic nuclide evidence indicates that the current ice surface is close to that first achieved at 3.5 ka (Ellsworths) or 2.5 ka (Pensacola) (Figure 8). The data also point to major ice flow direction change consistent with former flow across what is now the BIR. However, the data do not favour one or other hypothesis (relaxation vs readvance) concerning the history of ice changes in the last few thousand years. There is nothing from the geomorphology or from cosmogenic nuclide dating to rule out thinning to below the 3.5 ka (2.5 ka) level. On the other hand the geomorphological evidence of blue-ice moraine stability [Hein *et al.*, 2016a] and the early Holocene age of some blue ice itself [Winter *et al.*, 2016.] rules out extensive deglaciation with open fjords.

8. Hypotheses synthesis

On the face of it, the two scenarios for Late Holocene change in ice-sheet flow seem irreconcilable. One involves a gradual relaxation of the ice sheet, with ice dynamics and flow modified by the rerouting of basal water. The other relates to deglaciation upstream of the modern grounding line, followed by regrounding through postglacial uplift of relatively high ground to form ice rises. However, there is a consistent message, from multiple RES datasets and cosmogenic analyses, for major ice-flow dynamic change and ice-sheet reconfiguration within the SWSE, and wider WS sector, of the WAIS around the time of the mid-Holocene. Buckled RES layers within ice rises point to former enhanced flow where the ice now flows slowly; palaeo-flow stripes on the BIR indicate the former direction of that enhanced flow; and cosmogenic data reveal how upstream ice-sheet flow has changed direction from flowing East toward the BIR, to flowing West into the modern IIS. RES also reveals Raymond bumps within the KIR, HIR and BIR that are relatively recently formed, suggesting ice rise formation in the last few thousand years.

The major difference between the two scenarios is that, in one, the ice-sheet grounding line progressively retreated from its LGM position to its present grounding line, whereas in the other the grounding line retreated upstream of present limits and subsequently readvanced to the present. While numerical modelling demonstrates how this latter scenario is possible, there are no conclusive data for either.

While this disagreement might seem challenging to reconcile, the two scenarios have one important point of agreement beyond an acknowledgement of mid-Holocene ice sheet change; that is they can both accommodate a level of post-LGM isostatic uplift. In the former scenario, such uplift could lead to topographic influences on basal water flow and ice-sheet dynamics; in the latter it would lead to regrounding of an ice shelf and backfilling of grounded ice upstream. This agreement stems from the fact that the WS sector is a particularly

sensitive part of the ice sheet to relative sea level [Wright *et al.*, 2014]. Indeed the grounding line is known to oscillate by several kilometers each day as a consequence of tides lifting up otherwise grounded ice during high tide, and dropping it to the bed on low tide. This process has been observed over the BIR [Brunt *et al.*, 2011] and the FIS [Jeofry *et al.*, 2018b].

Given that the Robin Subglacial Basin is occupied by grounded ice that is relatively close to flotation [Ross *et al.*, 2012], if it were to deglaciade (i.e. the ice sheet were to lift off the bed) it is unlikely there would be any major isostatic signal. Hence, there may simply be no conclusive isostatic record in favour of one scenario.

It is also unlikely that RES, or more cosmogenic data from exposed surfaces, will provide a resolution to the problem. However, if we could obtain samples from key regions of the subglacial environment, and date them, we may be able to provide a solution. Conceptually, the best way to use cosmogenic nuclides to distinguish between the different scenarios is to drill the margins of some of the glaciers or ice streams where we have ice-sheet thinning histories. Retrieval of bedrock from below the margins will allow a test of the hypothesis that the ice has been thinner than present in the Holocene; any bedrock exposed in the Holocene and then re-covered by ice will still contain a significant inventory of *in situ* ^{14}C isotopes. If the bedrock had been exposed in a previous thinning/interglacial then the ^{14}C would have decayed (as its half-life = 5730 yrs). Drilling at various depths to find the boundary between ^{14}C -containing bedrock and that at lower elevation with no ^{14}C would enable determination of the minimum thickness reached. In addition, if subglacial access to the Robin Subglacial Basin or beneath the BIR is possible, where soft marine sediments deposited when the ice sheet was not present are thought to exist [Siebert *et al.*, 2016], it may be possible to date the material by radiocarbon methods - certainly obtaining a Holocene date from such a sample would be a significant piece of information in support of the readvance hypothesis. Drilling through the BIR, KIR and/or HIR would also enable us to retrieve subglacial sediments for radiocarbon analysis to determine if the bed was exposed to the ocean during the last few thousand years [Kingslake *et al.*, 2018]. Sampling the ice from such a borehole (either as a full core or a chippings from a rapid drilling system) may permit isotopic analysis to reveal signals of ice associated with either scenario; for example, if HIR was completely ungrounded during the Holocene its deep ice would have been deposited on the surface while on the main ice sheet at higher elevations than is plausible in an ice rise. This would leave an isotopic signature. Finally, sampling ice from the hypothesised relic basal crevasses and measuring borehole temperatures on HIR and BIR may be key to determining the grounding history of these crucial areas.

9. Summary

The WS sector of the WAIS is known to be one of the most sensitive regions of the ice sheet to ocean-driven melting and grounding line recession, with the SWSE being particularly vulnerable. However, despite the SWSE being at a threshold of change, owing to the present grounding line of IIS being perched at the top of a major steep reverse bed slope, satellite altimetry shows that the region is, at present, not experiencing significant change like in the Amundsen Bay region of WAIS. However, satellite imagery of surface flowstripes, coupled with RES evidence of buckled internal layers, and corroborated by cosmogenic

1002 dating of exposed surfaces, point to recent (mid-Holocene) and substantial ice-dynamic
1003 change in the SWSE.

1004 Two scenarios to explain this change have emerged. First, the ice-sheet gradually relaxed
1005 from its LGM position involving fast-flowing ice across the BIR. Because of ice-sheet
1006 thinning, water and ice flow were routed around what is now BIR to set up the ice sheet as
1007 we now see it. Alternatively, ice retreated inland of the present margin, forming an ice shelf
1008 over the RSB and the BIR/KIR/HIR, whereupon isostatic uplift led to regrounding over the ice
1009 rises, and the present flow regime to establish itself.

1010 While available glaciological information cannot distinguish between these scenarios, they
1011 do have some areas of commonality. First, all evidence points to mid-Holocene change to
1012 the flow and form of the SWSE. Second, both scenarios can accommodate postglacial uplift
1013 to drive either ice dynamic alteration on one hand, or grounding on the other. Third, it is also
1014 possible that both scenarios may have acted together, with uplift leading to regrounding and
1015 ice direction change alteration. Such a situation may account for buried crevasses within
1016 HIR, thought to be formed within an ice shelf and captured as a consequence of grounding,
1017 as well as the shear margin between IIS and BIR, which appears to be controlled solely by
1018 ice sheet thermodynamics and the supply of water, rather than topography. Fourth, we
1019 should appreciate that the SWSE experiences significant (>10 km) grounding line change as
1020 a consequence of tides, and much of the region is relatively close to the level of flotation
1021 now; hence migration of the grounding line upstream of modern limits could easily occur
1022 without much isostatic signal today.

1023 It is curious that the SWSE currently appears to show no sign of significant mass loss. The
1024 recent readvance hypothesis may be consistent with this, as the ice sheet would have
1025 effectively experienced expansion to its present limits. As ice-sheet modelling has shown,
1026 however, this is unlikely to make the sector more stable to the influx of warm ocean water; if
1027 this happened we still expect, under either scenario, for the SWSE to experience grounding
1028 line retreat across the RSB.

1029

1030 **Acknowledgements.** We thank David Small for drafting Figure 8. Funding was provided by
1031 the UK Natural Environment Research Council to MJS (NE/G013071/1), SSRJ
1032 (NE/R000824/1), DES (NE/1025840/1), JW (NE/I027576/1) and MJB (NE/F014260/1,
1033 NE/J008176/1, NE/K003674/1).

1034 **Data availability.** Ground-based ice-penetrating radar data can be obtained from the UK
1035 Polar Data Centre at <http://doi.org/99d>. A simple MATLAB script for viewing the raw
1036 radar data is also provided at this link.

1037

1038

1039 Figure Captions

1040 **Figure 1.** Ice and bed characteristics of the Weddell Sea region. A) Bed elevation [Fretwell
1041 et al., 2014]; B) Ice velocity [Rignot et al., 2011]; C) Ice surface elevation [Fretwell et al.,
1042 2014]. D) MODIS ice surface morphology [Haran et al., 2005; Scambos et al., 2007]. The
1043 modern grounding line [Haran et al., 2005] is shown as a grey line in A, B and C and the
1044 locations of ice-free regions (black areas) are shown in B and C; Inset shows figure location.
1045 Abbreviations are: Robin Subglacial Basin (RSB), Antarctic Peninsula (AP), Institute Ice
1046 Stream (IIS), Möller Ice Stream (MIS), Foundation Ice Stream (FIS), Rutford Ice Stream
1047 (RIS), Support Force Glacier (SFG), Recovery Glacier (RG), Slessor Glacier (SG), Carson
1048 Inlet Glacier (CI), Bungenstock Ice Rise (BIR), Berkener Island (BI), Henry Ice Rise (HIR),
1049 Korf Ice Rise (KIR), Skytrain Ice Rise (SIR), Pirrit Hills (PH), Martin-Nash Hills (MNH),
1050 Pagano Nunatak (PN), Pagano Shear Zone (PSZ), Horseshoe Valley (HV), Independence
1051 Hills (IH), Pensacola Mountains (PM), Patuxent Range (PR), Shackleton Range (ShR), Thiel
1052 Mountains (TM), Ellsworth Trough (ET), Heritage Range (HR), Sentinel Range (SR),
1053 Filchner Trough (FT), Thiel Trough (TT), Lake Ellsworth (SLE), Hercules Inlet (HI).

1054 **Figure 2.** Left hand side (a,c,e,g) are plan-view maps showing changes in ice thickness
1055 (colour scale) and grounding-line position (grey=start, black=end) over 2000 year model
1056 runs. Right-hand side (b,d,f,h) are plots of cumulative volume change against time for each
1057 of the ice stream catchments for the same experiment. Adapted from Wright et al. [2014].

1058 **Figure 3.** LGM ice extent and thickness change. Solid black line indicates Scenario MAX for
1059 LGM ice extent, dashed black line indicates Scenario MIN. Orange points indicate LGM ice
1060 thickness (m) difference relative to present [Bentley et al., 2014; Hein et al., 2016b; Johnson
1061 et al., 2019; Nichols et al., 2019]. GPS sites are shown by the blue triangles. Black areas are
1062 nunataks, grey line is the modern grounding line. The background is the Landsat Image
1063 Mosaic of Antarctica (LIMA) in combination with a hillshade of the Weddell Sea bathymetry
1064 from Bedmap2 [Fretwell et al., 2013].

1065 **Figure 4.** Radar investigations of the Ellsworth Trough. a) Landsat Image Mosaic of
1066 Antarctica (LIMA) [Bindshadler et al., 2008] showing surface features, as well as the
1067 location of radargram A-A', which is displayed in (c) and annotated in (d). The white line
1068 indicates the ASAID grounding line [Bindshadler et al., 2011]. (b) Rignot et al. [2017]
1069 MEaSUREs version 2 ice flow map shows enhanced flow speeds in major tributaries of the
1070 Institute Ice Stream. (c) SAR-processed radargram across the upper Ellsworth Trough.
1071 Arrows indicate processing artefacts, whilst processing steps prevent the upper 200 samples
1072 (~ 500 m) from being imaged. (d) Digitised interpretation of (c), highlighting the basal
1073 topography (brown), lower basal ice unit (B1) and upper basal ice unit (B2) (as described by
1074 [Winter et al., 2015]) as well as visible englacial stratigraphic layers (black). The secondary
1075 axis is the satellite-derived surface ice-flow speed from MEaSUREs version 2, shown in the
1076 figure as an orange line [Rignot et al., 2017].

1077 **Figure 5.** Schematic description of ice sheet change in the BIR region. (a) The current
1078 glaciological situation, with ice flowstripes noted. (b) LGM-type ice sheet, where northward
1079 flow of grounded ice from the WAIS interior dominates the region cross cutting the present
1080 day trunk of the Institute Ice Stream and across the BIR. (c) Mid Holocene Scenario A,
1081 where the Institute Ice Stream becomes active to the south of the BIR. (d) Mid Holocene
1082 Scenario B, where the grounding line has migrated upstream leaving the BIR region covered

by floating ice. (e) Later Holocene ice configuration, in which ice over the BIR becomes stagnant, thus leading to the present day ice-sheet configuration. This model works for both scenarios of ice sheet history. In the case of a retreat of grounded ice, the Institute Ice Stream activates as a consequence of ice sheet surface lowering and reorganization of the subglacial hydrological regime. In the case of regrounding of the BIR as a consequence of post glacial uplift, the IIS flows along its present direction because of stagnant ice across its northern border. Adapted from *Siegert et al.* [2013].

Figure 6. (a) MODIS image of the Bungenstock Ice Rise (BIR), with Institute Ice Stream (IIS) to the south, and Möller Ice Stream (MIS) to the East. The position of the RES transect in (b) is shown. Note the palaeo surface flowstripes trending SW-NE across BIR. (b) RES transect revealing (1) the shear margin between the BIR and IIS (dashed line); (2) the flat bed beneath BIR; (3) the steep reverse slope of IIS; (4) buckled RES layers beneath flat layers (solid arrow); and (5) a tilting englacial reflection emanating from the bed (dashed arrow).

Figure 7. Bed topography and englacial structure of Henry Ice Rise (HIR). (a) Bed topography of HIR from data published as part of the BEDMAP2 compilation [*Fretwell et al.*, 2013] and 700 km of ground-based ice-penetrating radar conducted in 2013/14 and 2014/15 [*Kingslake et al.*, 2018]. Yellow curves are flow lines. Colours show the elevation of the bed above sea level. (b) The normalized elevation of an isochronal internal layer. (c) A radargram showing the internal layer mapped in c and relic basal crevasses, along the line A-A' shown in c. (d) A close-up view of the buried relic crevasses. In (a) and (b) the background image is the MODIS Mosaic of Antarctica and the grounding line is shown in red. Adapted from *Kingslake et al.* [2018].

Figure 8. Cosmogenic nuclide measurements of Holocene ice sheet behaviour. (a) (i) Hypothetical age-elevation plot with two groups of scenarios. In both cases the ice sheet thins from a former (LGM) thicker configuration to reach the present ice sheet elevation in the Late Holocene. In scenario 'A' the ice sheet then stays at the present day level for a few ky to the present day. In scenario 'B' the ice sheet thins to below present elevations in the Late Holocene and re-thickens to the present-day. (b) Location map of the Holocene age-elevation cosmogenic profiles in the southern WS. (c) Age-elevation plot from the southern Ellsworth Mountains. Data compiled from *Bentley et al.* [2010] and *Hein et al.* [2016a; 2016b]. (d) Age-elevation plot from the Pensacola Mountains. Data compiled from *Balco et al.* [2016] and *Bentley et al.* [2017]. Two samples emerging from actively ice-cored moraines have been excluded from the plot because they may record buried ice ablation rather than ice sheet thinning.

Figure 9. Cross-sections of model-predicted ice thickness and bed deformation along a transect that crosses the Robin Subglacial Basin (RSB), Bungenstock Ice Rise (BIR), and Henry Ice Rise (HIR) at 5-kyr intervals during the last deglaciation. Model details are described in *Kingslake et al.* [2018]. The horizontal axis shows distance from the present-day grounding line (GL), units on the vertical axis are metres. The blue dotted line outlines the observed present-day configuration of the ice sheet and seafloor. (a) Last Glacial Maximum configuration, ice sheet grounded near continental shelf edge, seafloor isostatically-depressed by several hundred metres. (b) Grounding line located upstream of the RSB, ice shelf persists across the Weddell Sea, seafloor rebounding. (c) Rebound triggers ice shelf re-grounding and formation of the HIR. (d) Ongoing rebound and

1127 buttressing associated with the formation of the HIR results in formation of the BIR and
1128 grounding line readvance to present-day configuration. Adapted from *Kingslake et al.* [2018].
1129

1130 **References**

- 1131 A., G., Wahr, J., and Zhong, S. J. Computations of the viscoelastic response of a 3-D
1132 compressible Earth to surface loading: an application to Glacial Isostatic Adjustment in
1133 Antarctica and Canada. *Geophys. J. Int.* 192, 557–572 (2013).
- 1134 Anandakrishnan, S., and Alley, R.B. Stagnation of ice stream C, West Antarctica by water
1135 piracy. *Geophysical Research Letters*, 24, 265-268. (1997).
- 1136 Argus, D. F., Peltier, W. R., Drummond, R., and Moore, A. W. The Antarctica component of
1137 postglacial rebound model ICE-6G_C (VM5a) based on GPS positioning, exposure age
1138 dating of ice thicknesses, and relative sea level histories. *Geophys. J. Int.* 198, 537–563
1139 (2014).
- 1140 Arthern, R.J., Winebrenner, D.P., and Vaughan, D.G. Antarctic snow accumulation mapped
1141 using polarization of 4.3- cm wavelength microwave emission. *Journal of Geophysical*
1142 *Research: Atmospheres*, 111(D6). (2006).
- 1143 Asay-Davis, X. S., Cornford, S. L., Durand, G., Galton-Fenzi, B. K., Gladstone, R. M.,
1144 Gudmundsson, G. H., Hattermann, T., Holland, D. M., Holland, D., Holland, P. R., Martin, D.
1145 F., Mathiot, P., Pattyn, F., and Seroussi, H. Experimental design for three interrelated marine
1146 ice sheet and ocean model intercomparison projects: MISMIP v. 3 (MISMIP +), ISOMIP v. 2
1147 (ISOMIP +) and MISOMIP v. 1 (MISOMIP1), *Geosci. Model Dev.*, 9, 2471-2497,
1148 <https://doi.org/10.5194/gmd-9-2471-2016>. (2016).
- 1149 Balco, G., Todd, C., Huybers, K., Campbell, S., Vermeulen, M., Hegland, M., Goehring,
1150 B.M., and Hillebrand, T.R. Cosmogenic-nuclide exposure ages from the Pensacola
1151 Mountains adjacent to the Foundation Ice Stream, Antarctica, *American Journal of Science*,
1152 316, 6, 542-577. (2016).
- 1153 Balco, G. Contributions and unrealized potential contributions of cosmogenic-nuclide
1154 exposure dating to glacier chronology 1990–2010. *Quaternary Science Reviews*, 30(1–2), 3–
1155 27 (2011).
- 1156 Bamber, J.L., Vaughan, D.G., and Joughin, I. Widespread Complex Flow in the Interior of
1157 the Antarctic Ice Sheet. *Science* 2871248-1250. DOI: 10.1126/science.287.5456.1248.
1158 (2000).
- 1159 Bell, R.E., Ferraccioli, F., Creyts, T.T., Braaten, D., Corr, H., Das, I., Damaske, D., Frearson,
1160 N., Jordan, T., Rose, K., Studinger, M., and Wolovick, M., 2011, Widespread persistent
1161 thickening of the East Antarctic Ice Sheet by freezing from the base: *Science*, v. 331, p.
1162 1592-1595, doi: 10.1126/science.1200109.
- 1163 Bentley, M.J., Ó Cofaigh, C., Anderson, J.B., Conway, H., Davies, B., Graham, A.G.C.,
1164 Hillenbrand, C.-D., Hodgson, D.A., Jamieson, S.S.R., Larter, R.D., Mackintosh, A., Smith,
1165 J.A., Verleyen, E., Ackert, R.P., Bart, P.J., Berg, S., Brunstein, D., Canals, M., Colhoun,
1166 E.A., Crosta, X., Dickens, W.A., Domack, E., Dowdeswell, J.A., Dunbar, R., Ehrmann, W.,
1167 Evans, J., Favier, V., Fink, D., Fogwill, C.J., Glasser, N.F., Gohl, K., Golledge, N.R.,
1168 Goodwin, I., Gore, D.B., Greenwood, S.L., Hall, B.L., Hall, K., Hedding, D.W., Hein, A.S.,
1169 Hocking, E.P., Jakobsson, M., Johnson, J.S., Jomelli, V., Jones, R.S., Klages, J.P.,
1170 Kristoffersen, Y., Kuhn, G., Leventer, A., Licht, K., Lilly, K., Lindow, J., Livingstone, S.J.,

1171 Massé, G., McGlone, M.S., McKay, R.M., Melles, M., Miura, H., Mulvaney, R., Nel, W.,
1172 Nitsche, F.O., O'Brien, P.E., Post, A.L., Roberts, S.J., Saunders, K.M., Selkirk, P.M., Simms,
1173 A.R., Spiegel, C., Stollendorf, T.D., Sugden, D.E., van der Putten, N., van Ommen, T.,
1174 Verfaillie, D., Vyverman, W., Wagner, B., White, D.A., Witus, A.E. & Zwartz, D. A
1175 community-based geological reconstruction of Antarctic Ice Sheet deglaciation since the
1176 Last Glacial Maximum. *Quaternary Science Reviews*. 100, 1-9. (2014).

1177 Bentley, M.J., Fogwill, C.J., Le Brocq, A.M., Hubbard, A.L., Sugden, D.E., Dunai, T.J., and
1178 Freeman, S.P.H.T. Deglacial history of the West Antarctic Ice Sheet in the Weddell Sea
1179 embayment: constraints on past ice volume and change. *Geology*, 38, 411-414,
1180 doi:<https://doi.org/10.1130/G30754.1>. (2010).

1181 Bentley, M.J., Fogwill, C.J., Le Brocq, A.M., Hubbard, A.L., Sugden, D.E., Dunai, T. &
1182 Freeman, S.P.H.T., 2011. Deglacial history of the West Antarctic Ice Sheet in the Weddell
1183 Sea embayment: Constraints on past ice volume change: REPLY, *Geology*, 39, e240,
1184 10.1130/G32140Y.1

1185 Bentley, M.J., Hein, A.S., Sugden, D.E., Whitehouse, P.L., Shanks, R., Xu, S., and Freeman,
1186 S.P.H.T. Deglacial history of the Pensacola Mountains, Antarctica from glacial
1187 geomorphology and cosmogenic nuclide surface exposure dating, *Quaternary Science*
1188 *Reviews*, v. 158, pp. 58-76. (2017).

1189 Bingham, R., and Siegert, M.J. Airborne radio-echo sounding over polar ice masses. *Journal*
1190 *of Environmental & Engineering Geophysics*, 12, 47-62. (2007).

1191 Bingham, R.G., Siegert, M.J., Blankenship, D.D., and Young, D.A. Organized flow from the
1192 South Pole to the Filchner-Ronne ice shelf: an assessment of balance velocities in interior
1193 East Antarctica using radio-echo sounding data. *Journal of Geophysical Research*, 112,
1194 F03S26, doi:10.1029/2006JF000556. (2007).

1195 Bindschadler, R.A., Vornberger, P., Flemming, A., Fox, A., Mullins, J., Binnie, D., Paulsen,
1196 S.J., Granneman, B., and Gorodetzky, D. The Landsat image mosaic of Antarctica. *Remote*
1197 *Sensing of the Environment*, 112, 4214–4226, doi: 0.1016/j.rse.2008.07.006. (2008).
1198

1199 Bindschadler, R.A., Vaughan, D.G., and Vornberger, P. Variability of basal melt beneath the
1200 Pine Island Glacier ice shelf, West Antarctica. *Journal of Glaciology*, 57(204), 581– 595, doi:
1201 10.3189/002214311797409802. (2011).
1202

1203 Bons, P.D., Jansen, D., Mundel, F., Bauer, C.C., Binder, T., Eisen, O., Jessell, M.W.,
1204 Llorens, M-G., Steinbach, F., Steinhage, D., and Weikusat, I. Converging flow and
1205 anisotropy cause large-scale folding in Greenland's ice sheet: *Nature Communications*, 7,
1206 11427, doi: 10.1038/ncomms11427. (2016).

1207 Bradley, S.L., Hindmarsh, R.C.A., Whitehouse, P.L., Bentley, M.J., and King, M.A. Low post-
1208 glacial rebound rates in the Weddell Sea due to Late Holocene ice-sheet readvance . *Earth*
1209 *and Planetary Science Letters*, 414, 79-9, doi:10.1016/j.epsl.2014.12.039. (2015).

1210 Briggs, R. D., Pollard, D., and Tarasov, L. A data-constrained large ensemble analysis of
1211 Antarctic evolution since the Eemian. *Quat. Sci. Rev.* 103, 91–115 (2014).

1212 Brisbourne, A.M., Martín, C., Smith, A.M., Baird, A.F., Kendall, J.M., and Kingslake, J.
1213 Constraining recent ice flow history at Korff Ice Rise, West Antarctica, using radar and
1214 seismic measurements of ice fabric. *Journal of Geophysical Research: Earth Surface*, 124,
1215 175-194, doi: 10.1029/2018JF004776 (2019).

1216 Brisbourne, A.M., C. Martín, A.M. Smith, A.F. Baird, J.M. Kendall & J. Kingslake
1217 Constraining Recent Ice Flow History at Korff Ice Rise, West Antarctica, Using Radar and
1218 Seismic Measurements of Ice Fabric. *J. Geophys. Res. Earth Surf.*, 124(1), 175-194. (2019).

1219 Brunt, K.E., Fricker, H.A., and Padman, L. Analysis of ice plains of the Filchner–Ronne Ice
1220 Shelf, Antarctica, using ICESat laser altimetry, *J. Glaciol.* 57, 965-975. (2011).

1221 Bueler, E., Lingle, C., and Brown, J. Fast computation of a viscoelastic deformable Earth
1222 model for ice-sheet simulations. *Annals of Glaciology*, 46, 97–105. (2007).

1223 Catania, G. A., Scambos, T.A., Conway, H., and Raymond, C.F. Sequential stagnation of
1224 Kamb Ice Stream, West Antarctica, *Geophys. Res. Lett.*, 33, L14502,
1225 doi:10.1029/2006GL026430. (2006).

1226 Catania, G.A., Scambos, T.A., Conway, H., and Raymond, C.F. Sequential stagnation of
1227 Kamb Ice Stream, West Antarctica. *Journal of Glaciology*, Vol. 58, No. 210, 2012 doi:
1228 10.3189/2012JoG11J219. (2012).

1229 Clark, P.U., 2011, Deglacial history of the West Antarctic Ice Sheet in the Weddell Sea
1230 embayment: Constraints on past ice volume change: Comment, *Geology*,
1231 doi:10.1130/G31533C.1.

1232 Conway, H., Hall, B.L., Denton, G.H., Gades, A.M., and Waddington, E.D. Past and future
1233 grounding-line retreat of the West Antarctic Ice Sheet. *Science*, 286, 280-283. (1999).

1234 Cornford, S.L., Martin, D.F., Graves, D.T., Ranken, D.F., Le Brocq, A.M., Gladstone, R.M.,
1235 Payne, A.J., Ng, E.G., and Lipscomb, W.H. Adaptive mesh, finite volume modeling of marine
1236 ice sheets. *Journal of Computational Physics*, 232, 529-549. (2013).

1237 Curtis, M. L. Tectonic history of the Ellsworth Mountains, West Antarctica: reconciling a
1238 Gondwana enigma. *Geological Society of America Bulletin*, 113, 939–958. (2001).

1239 Dalziel and Elliot. West Antarctica: Problem Child of Gondwanaland. *Tectonics*, 1, 3-19. doi:
1240 10.1029/TC001i001p00003. (1982).

1241 de Boer, B., Stocchi, P., Whitehouse, P. L., and van de Wal, R. S. W.: Current state and
1242 future perspectives on coupled ice-sheet– sea-level modelling, *Quaternary Sci. Rev.*, 169,
1243 13–28, <https://doi.org/10.1016/j.quascirev.2017.05.013> . (2017).

1244 Dowdeswell, J.A., and Evans, S. Investigations of the form and flow of ice sheets and
1245 glaciers using radio-echo sounding. *Reports on Progress in Physics*. 67, 1821–1861 (2004).

1246 Engels, O., Gunter, B. C., Riva, R. E. M., and Klees, R. Separating geophysical signals
1247 using GRACE and high-resolution data: A case study in Antarctica, *Geophysical Research*
1248 *Letters*, 45, 12,340–12,349. (2018).

1249 Favier, L., and Pattyn, F. Antarctic ice rise formation, evolution, and stability. *Geophys. Res.*
1250 *Lett.*, 42 , 4456–4463, doi:10.1002/2015GL064195. (2015).

1251 Fretwell, P. et al. Bedmap2: improved ice bed, surface and thickness datasets for Antarctica.
1252 *The Cryosphere*, 7, 375–393. doi:10.5194/tc-7-375-2013 (2013).

1253 Goehring, B.M., Schaefer, J.M., Schluechter, C., Lifton, N.A., Finkel, R.C., Jull, A.J.T., Akcar,
1254 N., and Alley, R.B. The Rhone Glacier was smaller than today for most of the Holocene,
1255 *Geology*, 39, 7, pp. 679-682. (2011).

1256 Goehring, B.M., Balco, G., Todd, C., Moening-Swanson, I., Nichols, K. Late-glacial
1257 grounding line retreat in the northern Ross Sea, Antarctica, *Geology*, 47, 291-294. doi:
1258 10.1130/G45413.1 (2019)

1259 Golledge, N. R. et al. Antarctic contribution to meltwater pulse 1A from reduced Southern
1260 Ocean overturning. *Nature Communications*, 5, 5107 (2014).

1261 Gomez, N., Mitrovica, J.X., Huybers, P., and Clark, P.U. Sea level as a stabilizing factor for
1262 marine-ice-sheet grounding lines. *Nature Geoscience*, 3, 850–853 (2010)

1263 Gomez, N., Pollard, D., and Mitrovica, J. X. A 3-D coupled ice sheet-sea level model applied
1264 to Antarctica through the last 40 ky. *Earth Planet. Sci. Lett.* 384, 88–99 (2013).

1265 Gomez, N., Pollard, D., and Holland, D. Sea-level feedback lowers projections of future
1266 Antarctic Ice-Sheet mass loss. *Nature Communications*, 6, 8798 (2015).

1267 Gomez, N., Latychev, K., and Pollard, D. A coupled ice sheet-sea level model incorporating
1268 3D Earth structure: Variations in Antarctica during the last deglacial retreat. *J. Clim.* 31,
1269 4041–4054 (2018).

1270 Gunter, B. C. et al. Empirical estimation of present-day Antarctic glacial isostatic adjustment
1271 and ice mass change. *Cryosphere* 8, 743–760 (2014).

1272 Haran, T., J. Bohlander, T. Scambos, T. Painter, and M. Fahnestock. *MODIS Mosaic of*
1273 *Antarctica 2003-2004 (MOA2004) Image Map*. [indicate subset used].Boulder, Colorado
1274 USA: National Snow and Ice Data Center. <http://dx.doi.org/10.7265/N5ZK5DM5> (2005)

1275 Hay, C. C. et al. Sea-level fingerprints in a region of complex Earth structure: the case of
1276 WAIS. *J. Clim.* 30, 1881–1892 (2017).

1277 Hein, A.S., Woodward, J., Marrero, S.M., Dunning, S.A., Steig, E.J., Freeman, S.P.H.T.,
1278 Stuart, F.M., Winter, K., Westoby, M.J., and Sugden, D.E. Evidence of the stability of the
1279 West Antarctic Ice Sheet divide for 1.4 million years, *Nature Communications*, v.7, 10325.
1280 DOI: 10.1038/ncomms10325. (2016a).

1281 Hein, A.S., Marrero, S.M., Woodward, J., Dunning, S.A., Winter, K., Westoby, M.J.,
1282 Freeman, S.P.H.T., Shanks, R.P., and Sugden, D.E. Mid-Holocene pulse of thinning in the
1283 Weddell Sea sector of the West Antarctic ice sheet, *Nature Communications*, v. 7, 12511.
1284 DOI: 10.1038/ncomms12511. (2016b).

1285 Hellmer, H.H., Kauker, F., Timmermann, R., Determann, J., and Rae, J. Twenty-first-century
 1286 warming of a large Antarctic ice-shelf cavity by a redirected coastal current. *Nature*, 485,
 1287 225-228. (2012).

1288 Hillenbrand, C.D., Bentley, M.J., Stollendorf, T.D., Hein, A.S., Kuhne, G., Graham, A.G.C.,
 1289 Gogwill, C.J., Kristoffersen, Y., Smith, J.A., Anderson, J.B., Larter, R.D., Melles, M.,
 1290 Hodgson, D.A., Mulvaney, R., and Sugden, D.E. *Quaternary Science Reviews*, 100, 111-
 1291 136. (2014).

1292 Holschuh, N., Christianson, K., Conway, H., Jacobel, R. W., and Welch, B. C.: Persistent
 1293 tracers of historic ice flow in glacial stratigraphy near Kamb Ice Stream, West Antarctica, *The*
 1294 *Cryosphere*, 12, 2821-2829, <https://doi.org/10.5194/tc-12-2821-2018>. (2018).

1295 IPCC, 2013. *Climate Change 2013: The Physical Science Basis. Contribution of Working*
 1296 *Group I to the Fifth Assessment Report of the Intergovernmental Panel on Climate Change*
 1297 [Stocker, T.F., D. Qin, G.-K. Plattner, M. Tignor, S.K. Allen, J. Boschung, A. Nauels, Y. Xia,
 1298 V. Bex and P.M. Midgley (eds.)]. Cambridge University Press, Cambridge, United Kingdom
 1299 and New York, NY, USA, 1535 pp.

1300 Ivins, E. R. et al. Antarctic contribution to sea-level rise observed by GRACE with improved
 1301 GIA correction. *J. Geophys. Res.: Solid Earth* 118, 3126–3141 (2013).

1302 Jeofry, H., Ross, N., Corr, H.F.J., Li, J., Morlighem, M., Gogineni, P., and Siegert, M.J. A
 1303 new digital elevation model for the Weddell Sea sector of the West Antarctic Ice Sheet. *Earth*
 1304 *System Science Data*, 10, 711–725 doi: 10.5194/essd-10-711-2018 (2018a).

1305 Jeofry, H., Ross, N., Le Brocq, A., Graham, A., Li, J., Gogineni, P., Morlighem, M., Jordan,
 1306 T., and Siegert, M.J. Hard rock landforms generate 130 km ice shelf channels through water
 1307 focusing in basal corrugations. *Nature Communications*, 9, 4576 doi:10.1038/s41467-018-
 1308 06679-z (2018b).

1309 Johnson, J.S., Nichols, K.A., Goehring, B.M., Balco, G., and Schaefer, J.M. Abrupt mid-
 1310 Holocene ice loss in the western Weddell Sea Embayment of Antarctica. *Earth and*
 1311 *Planetary Science Letters*, 518 127–135 doi:10.1016/j.epsl.2019.05.002 (2019).

1312 Jordan, T.A., Ferraccioli, F., Ross, N., Corr, H.F.J., Leat, P.T., Bingham, R.G., Rippin, D.M.,
 1313 Le Brocq, A., and Siegert, M.J. Inland extent of the Weddell Sea Rift imaged by new
 1314 aerogeophysical data. *Tectonophysics*, 585, 137-160. doi.org/10.1016/j.tecto.2012.09.010
 1315 (2013).

1316 Jordan, T.A., Martin, C., Ferraccioli, F., Matsuoka, K., Corr, H., Forsberg, R., Olesen, A., and
 1317 Siegert, M.J. Geothermal anomaly facilitates ice-flow variability in East Antarctic Ice Sheet
 1318 interior. *Scientific Reports*. 8:16785 (2018). doi:10.1038/s41598-018-35182-0 (2018).

1319 Joughin, I., Smith, B.E., and Medley, B. Marine Ice Sheet Collapse Potentially Under Way for
 1320 the Thwaites Glacier Basin, West Antarctica. *Science*, 344, 735-738 doi:
 1321 10.1126/science.1249055. (2014).

1322 Kingslake, J., Martín, C., Arthern, R.J., Corr, H.F.J., and King, E.C. Ice-flow reorganization in
 1323 West Antarctica 2.5 kyr ago dated using radar-derived englacial flow velocities. *Geophys.*
 1324 *Res. Lett.*, 43, 9103–9112, doi:10.1002/2016GL070278. (2016).

1325 Kingslake, J., Scherer, R.P., Albrecht, T., Coenen, J., Powell, R.D., Reese, R., Stansell,
 1326 N.D., Tulaczyk, S., Wearing, M.G. and Whitehouse, P.L., 2018. Extensive retreat and re-
 1327 advance of the West Antarctic Ice Sheet during the Holocene. *Nature*, 558(7710), p.430.

1328 Konrad, H., Sasgen, I., Pollard, D. and Klemann, V. Potential of the solid-Earth response for
 1329 limiting long-term West Antarctic Ice Sheet retreat in a warming climate. *Earth Planet. Sci.*
 1330 *Lett.* 432, 254–264 (2015).

1331 Lal, D. Cosmic-ray labelling of erosion surfaces – in situ nuclide production-rates and
 1332 erosion models, *Earth and Planetary Science Letters*, v. 104, 2-4, pp. 424-439. (1991).

1333 Le Brocq, A.M., Bentley, M.J., Hubbard, A., Fogwill, C.J., Sugden, D.E., and Whitehouse,
 1334 P.L.. Reconstructing the Last Glacial Maximum ice sheet in the Weddell Sea embayment,
 1335 Antarctica, using numerical modelling constrained by field evidence. *Quaternary Science*
 1336 *Reviews*, 30, 2422-2432. doi:10.1016/j.quascirev.2011.05.009 (2011).

1337 Le Brocq, A., Ross, N., Griggs, J., Bingham, R., Corr, H., Ferroccioli, F., Jenkins, A., Jordan,
 1338 T., Payne, A., Rippin, D. and Siegert, M.J. Ice shelves record the history of channelised flow
 1339 beneath the Antarctic ice sheet. *Nature Geoscience*, 6, 945–948 doi:10.1038/ngeo1977.
 1340 (2013).

1341 Mackintosh, A., White, D., Fink, D., Gore, D.B., Pickard, J., and Fanning, P.C. Exposure
 1342 ages from mountain dipsticks in Mac. Robertson Land, East Antarctica, indicate little change
 1343 in ice-sheet thickness since the Last Glacial Maximum, *Geology*, v. 35, 6, pp. 551-554.
 1344 (2007).

1345 Maris, M. N. A., de Boer, B., Ligtenberg, S. R. M., Crucifix, M., van de Berg, W. J., and
 1346 Oerlemans, J.: Modelling the evolution of the Antarctic ice sheet since the last interglacial,
 1347 *The Cryosphere*, 8, 1347-1360, <https://doi.org/10.5194/tc-8-1347-2014>. (2014).

1348 Martín, C., Hindmarsh, R.C.A., and Navarro, F.J.. On the effects of divide migration, along-
 1349 ridge flow, and basal sliding on isochrones near an ice divide, *J. Geophys. Res.*, 114,
 1350 F02006, doi:10.1029/2008JF001025. (2009).

1351 Martín, C., Hindmarsh, R.C.A., and Navarro, F.J.. Dating ice flow change near the flow
 1352 divide at Roosevelt Island, Antarctica, by using a thermomechanical model to predict radar
 1353 stratigraphy, *J. Geophys. Res.*, 111, F01011, doi:10.1029/2005JF000326. (2006).

1354 Martin-Espanol, A. et al. Spatial and temporal Antarctic Ice Sheet mass trends, glacio-
 1355 isostatic adjustment, and surface processes from a joint inversion of satellite altimeter,
 1356 gravity, and GPS data. *J. Geophys. Res. Earth Surf.* 121, 182–200 (2016a).

1357 Martín-Español, A. et al. An assessment of forward and inverse GIA solutions for Antarctica.
 1358 *J. Geophys. Res. Solid Earth* 121, 6947–6965 (2016b).

1359 Matsuoka, K., Hindmarsh, R.C.A., Moholdt, G., Bentley, M.J., Pritchard, H.D., Brown, J.,
 1360 Conway, H., Drews, R., Durand, G., Goldberg, D., Hattermann, T., Kingslake, J., Lenaerts,
 1361 J.T.M., Matrin, C., Mulvney, R., Nicholls, K.W., Pattyn, F., Ross, N., Scambos, R. and
 1362 Whitehouse, P.L. Antarctic ice rises and rumpled: their properties and significance for ice-
 1363 sheet dynamics and evolution. *Earth-Science Reviews*, 150, 724-745,
 1364 doi:10.1016/j.earscirev.2015.09.004 (2015).

1365 McConnell, R. K. Isostatic Adjustment in a Layered Earth. *Journal of Geophysical Research*
1366 70, doi:10.1029/JZ070i020p05171 (1965).

1367 Mitrovica, J., and Forte, A., A new inference of mantle viscosity based upon joint inversion of
1368 convection and glacial isostatic adjustment data. *Earth Planet. Sci. Lett.* 225, 177–189.
1369 (2004).

1370 Morse, D.L., Waddington, E.D. and Steig, E.J. Ice age storm trajectories inferred from radar
1371 stratigraphy at Taylor Dome, Antarctica. *Geophysical Research Letters*, 25 (17), 3383-3386.
1372 (1998).

1373 Mouginot J., Rignot E., Scheuchl B., and Millan R. Comprehensive annual ice sheet velocity
1374 mapping using Landsat-8, Sentinel-1, and RADARSAT-2 data. *Remote Sens* 9:364–1370
1375 (2017).

1376 Mulvaney, R et al. 1000-year ice core records from Berkner Island, Antarctic. *Annals of*
1377 *Glaciology*, 35, 45-51, doi: 10.3189/172756402781817176 (2002).

1378 Nield, G.A., Whitehouse, P.L., van der Wal, B., Blank, B., O'Donnell, P. and Stuart, G.W.
1379 The impact of lateral variations in lithospheric thickness on glacial isostatic adjustment in
1380 West Antarctica. *Geophys. J. Int.* 2, 811–824, doi: 10.1093/gji/ggy158 (2018).

1381 Pollard, D., Gomez, N. and DeConto, R. M. Variations of the Antarctic Ice Sheet in a coupled
1382 ice sheet-Earth-sea level model: sensitivity to viscoelastic Earth properties. *J. Geophys. Res.*
1383 *Earth Surf.* 122, 2124–2138 (2017).

1384 Raymond, C.F. Deformation in the vicinity of ice divides. *Journal of Glaciology*, 29, 357–
1385 373.(1983)

1386 Rignot, E., Mouginot, J., and Scheuchl, B. MEaSURES InSAR- based Antarctica ice velocity
1387 map, version 2, Boulder, Colorado USA, NASA National Snow and Ice Data Center
1388 Distributed Active Archive Center. doi:10.5067/D7GK8F5J8M8R (2011).

1389 Rignot, E., Mouginot, J., Scheuchl, B., van den Broeke, M., van Wessem, M.J., and
1390 Morlighem, M. Four decades of Antarctic Ice Sheet mass balance from 1979–2017. *PNAS*.
1391 116, 1095-1103. Doi: 10.1073/pnas.1812883116

1392 Rose, K.C., Ross, N., Bingham, R.G., Corr, H.F.J., Ferraccioli, F., Jordan, T.A., Le Brocq, A.,
1393 Rippin, D.M. and Siegert, M.J. A temperate former West Antarctic ice sheet suggested by an
1394 extensive zone of bed channels. *Geology*, 42, 971-974. doi:10.1130/G35980.1 (2014).

1395 Rose, K.C., Ross, N., Jordan, T.A., Bingham, R.G., Corr, H., Ferraccioli, F., Le Brocq, A.,
1396 Rippin, D.M., and Siegert, M.J. Ancient pre-glacial erosion surfaces preserved beneath the
1397 West Antarctic ice sheet. *Earth Surface Dynamics*, 3, 139-152. doi:10.5194/esurf-3-139-
1398 2015 (2015).

1399 Rosier, S.H.R., Hofstede, C., Brisbourne, A.M., Hattermann, R., Nicholls, K.W., Davis,
1400 P.E.D., Anker, P.G.D., Hillenbrand, C-D., Smith, A.M., and Corr, H.F.J. A new bathymetry for
1401 the southeastern Filchner-Ronne Ice Shelf: implications for modern oceanographic
1402 processes and glacial history. *Journal of Geophysical Research*, 7, 4610-4623.
1403 doi:10.1029/2018JC013982, (2018).

1404 Ross, N., Bingham, R.G., Corr, H., Ferraccioli, F., Jordan, T.A., Le Brocq, A., Rippin, D.M.,
 1405 Young, D., Blankenship, D.D. and Siegert, M.J. Steep reverse bed slope at the grounding
 1406 line of the Weddell Sea sector in West Antarctica Nature Geoscience, 5, 393 - 396. doi:
 1407 10.1038/ngeo1468, (2012).

1408 Ross, N. and Siegert, M. Concentrated englacial shear over rigid basal ice, West Antarctica:
 1409 Implications for modeling and ice sheet flow. Geophys. Res. Abstr., 16, EGU2014–5568.
 1410 (2014).

1411 Ross, N., Jordan, T.A., Bingham, R.G., Corr, H.F.J., Ferraccioli, F., Le Brocq, A., Rippin,
 1412 D.M., Wright, A.P., and Siegert, M.J. The Ellsworth Subglacial Highlands: inception and
 1413 retreat of the West Antarctic Ice Sheet. Geological Society of America Bulletin. 126, 3-15 doi:
 1414 10.1130/B30794.1 (2014).

1415 Ross, N., Siegert, M.J., Woodward, J., Smith, A.M., Corr, H.F.J., Bentley, M.J., Hindmarsh,
 1416 R.C.A., King, E.C., and Rivera, A. Holocene stability of the Pine Island Glacier-Weddell Sea
 1417 ice divide, West Antarctica. Geology, 39(10), 935–938 (2011).

1418 Sasgen, I. et al. Joint inversion estimate of regional glacial isostatic adjustment in Antarctica
 1419 considering a lateral varying Earth structure (ESA STSE Project REGINA). Geophys. J. Int.
 1420 211, 1534–1553 (2017).

1421 Scambos, T., T. Haran, M. Fahnestock, T. Painter, and J. Bohlander. MODIS-based Mosaic
 1422 of Antarctica (MOA) Data Sets: Continent-wide Surface Morphology and Snow Grain Size.
 1423 *Remote Sensing of Environment*, 111(2): 242-257.
 1424 <http://dx.doi.org/10.1016/j.rse.2006.12.020> (2007).

1425 Shen, W. et al. The crust and upper mantle structure of central and West Antarctica from
 1426 Bayesian inversion of Rayleigh wave and receiver functions. J. Geophys. Res. doi:
 1427 10.1029/2017JB015346 (2018).

1428 Shepherd, A., and 78 others. Mass balance of the Antarctic ice sheet from 1992 to 2017.
 1429 Nature, 58, 219-222. doi:10.1038/s41586-018-0179-y. (2018).

1430 Siegert, M.J. *Ice sheets and Late Quaternary environmental change*. John Wiley,
 1431 Chichester, UK, 231pp. (2001).

1432 Siegert, M.J. and Leysinger Vieli, G.J.M.C. Late glacial history of the Ross Sea sector of the
 1433 West Antarctic ice sheet: evidence from englacial layering at Talos Dome, East Antarctica.
 1434 Journal of Environmental and Engineering Geophysics, 12, 63-67 (2007).

1435 Siegert, M.J. On the origin, nature and uses of Antarctic ice-sheet radio-echo layering.
 1436 Progress in Physical Geography, 23, 159-179, (1999).

1437 Siegert, M.J. and Payne, A.J. Past rates of accumulation in central West Antarctica.
 1438 Geophysical Research Letters, 31, (12), L12403 10.1029/2004GL020290. (2004).

1439 Siegert, M.J., Ross, N., Corr, H., Kingslake, J., and Hindmarsh, R. Late Holocene ice-flow
 1440 reconfiguration in the Weddell Sea sector of West Antarctica. Quaternary Science Reviews,
 1441 78, 98-107 doi: 10.1016/j.quascirev.2013.08.003 (2013).

1442 Siegert, M.J., Ross, N., Li, J., Schroeder, D., Rippin, D., Ashmore, D., Bingham, R., and
 1443 Gogineni, P. Controls on the onset and flow of Institute Ice Stream, West Antarctica. *Annals*
 1444 *of Glaciology*, 57, 19-24 10.1017/aog.2016.17 (2016).

1445 Siegert, M.J., Welch, B., Morse, D., Vieli, A., Blankenship, D.D., Joughin, I., King E.C.,
 1446 Leysinger Vieli, G.J.M.C., Payne, A.J., and Jacobel, R. Ice flow direction change in interior
 1447 West Antarctica. *Science*, 305, 1948-1951. 10.1126/science.1101072 (2004b).

1448 Siegert, M.J., Clarke, R.J., Mowlem, M., Ross, N., Hill, C.S., Tait, A., Hodgson, D., Parnell,
 1449 J., Tranter, M., Pearce, D., Bentley, M., Cockell, C., Tsaloglou, M.N., Smith, A., Woodward,
 1450 J., Brito, M.P. and Waugh, E. Clean access, measurement and sampling of Ellsworth
 1451 Subglacial Lake: a method to explore deep Antarctic subglacial lake environments. *Reviews*
 1452 *of Geophysics*, 50, RG1003, doi:10.1029/2011RG000361 (2012).

1453 Smith, B.E., Fricker, H.A., Joughin, I.R., and Tulaczyk, S. An inventory of active subglacial
 1454 lakes in Antarctica detected by ICESat (2003-2008). *Journal of Glaciology*, **55** (129), 573-
 1455 595. (2009).

1456 Spector, P., Stone, J., Pollard, D., Hillenbrand, T., Lewis, C. and Gombiner, J. West
 1457 Antarctic sites for subglacial drilling to test for past ice-sheet collapse. *The Cryosphere* 12,
 1458 2741-2757. <https://doi.org/10.5194/tc-12-2741-2018> (2018).

1459 Stone, J.O., Balco, G.A., Sugden, D.E., Caffee, M.W., Sass, L.C., Cowdery, S.G. and
 1460 Siddoway, C. Holocene deglaciation of Marie Byrd Land, West Antarctica, *Science*, v. 299,
 1461 5603, pp. 99-102. (2003).

1462 Sugden D.E. and Jamieson, S.S.R. The pre-glacial landscape of Antarctica. *Scottish*
 1463 *Geographical Journal*, 134, 203-223, <https://doi.org/10.1080/14702541.2018.1535090>
 1464 (2018).

1465 Sugden, D.E., Hein, A.S., Woodward J., Marrero, S.M., Rodés, A., Dunning, S.A., Stuart,
 1466 F.M., Freeman, P.H.T., Winter, K., Westoby, M.J. The million-year evolution of the glacial
 1467 trimline in the southernmost Ellsworth Mountains, Antarctica. *Earth and Planetary Science*
 1468 *Letters*, 469, 42-52. <https://doi.org/10.1016/j.epsl.2017.04.006> and
 1469 <https://doi.org/10.1016/j.epsl.2018.08.053> (2017).

1470 van der Wal, W., Whitehouse, P.L. and Schrama, E.J.O. Effect of GIA models with 3D
 1471 composite mantle viscosity on GRACE mass balance estimates for Antarctica. *Earth Planet.*
 1472 *Sci. Lett.* 414, 134–143 (2015).

1473 van Wessem, J.M., Jan Van De Berg, W., Noël, B.P., Van Meijgaard, E., Amory, C.,
 1474 Birnbaum, G., Jakobs, C.L., Krüger, K., Lenaerts, J., Lhermitte, S. and Ligtenberg, S.R.
 1475 Modelling the climate and surface mass balance of polar ice sheets using RACMO2: Part 2:
 1476 Antarctica (1979-2016). *Cryosphere*, 12(4), pp.1479-1498. (2018).

1477 W.A.I.S. Drilling Project Members. Onset of deglacial warming in West Antarctica driven by
 1478 local orbital forcing, *Nature*, 500, 440-444. (2013).

1479 White, D., Fulop, R.H., Bishop, P., Mackintosh, A. and Cook, G. Can in-situ cosmogenic C-
 1480 14 be used to assess the influence of clast recycling on exposure dating of ice retreat in
 1481 Antarctica? *Quaternary Geochronology*, v. 6, 3-4, pp. 289-294. (2011).

1482 Whitehouse, P. L., Bentley, M. J. and Le Brocq, A. M. A deglacial model for Antarctica:
 1483 geological constraints and glaciological modelling as a basis for a new model of Antarctic
 1484 glacial isostatic adjustment. *Quat. Sci. Rev.* 32, 1–24 (2012a).

1485 Whitehouse, P.L., Bentley, M.J., Milne, G.A., King, M.A. and Thomas, I.D. A new glacial
 1486 isostatic adjustment model for Antarctica: calibrated and tested using observations of relative
 1487 sea-level change and present-day uplift rates. *Geophysical Journal International*, 190, 1464–
 1488 1482. doi:10.1111/j.1365-246X.2012.05557.x (2012b).

1489 Whitehouse, P. L., Bentley, M.J., Vieli, A., Jamieson, S.S.R., Hein, A.S. and Sugden, D.E.
 1490 Controls on Last Glacial Maximum ice extent in the Weddell Sea embayment, Antarctica, *J.*
 1491 *Geophys. Res. Earth Surf.*, 122, 371–397, doi:10.1002/2016JF004121. (2017).

1492 Whitehouse, P. L. Glacial isostatic adjustment modelling: historical perspectives, recent
 1493 advances, and future directions. *Earth Surf. Dynam* 6, 401–429 (2018).

1494 Whitehouse, P.L., Gomez, N., King, M.A. and Wiens, D.A. Solid Earth change and the
 1495 evolution of the Antarctic Ice Sheet. *Nature Communications*, 10:503, (2019).

1496 Winter, K., Woodward, J., Ross, N., Dunning, S.A., Corr, H.F.J., Bingham, R.J. and Siegert,
 1497 M.J. Airborne radar evidence for tributary flow switching in the Institute Ice Stream upper
 1498 catchment, West Antarctica: implications for ice sheet configuration and dynamics. *Journal*
 1499 *of Geophysical Research*, 120, 1611-1625. doi:10.1002/2015JF003518 (2015).

1500 Winter, K., Woodward, J., Dunning, S.A., Turney, C.S.M., Fogwill, C.J., Hein, A.S., Golledge,
 1501 N.R., Bingham, R.G., Marrero, S.M., Sugden, D.E. and Ross, N. Assessing the continuity of
 1502 the blue ice climate record at Patriot Hills, Horseshoe Valley, West Antarctica. *Geophysical*
 1503 *Research Letters*, 43 (5), 2019-2026. doi:10.1002/2015GL066476 (2016).

1504 Winter, K., Ross, N., Ferraccioli, F., Jordan, T., Corr, H.F.J., Forsberg, R., Matsuoka, K.,
 1505 Olesen, A.V. and Casal, T.G. Topographic steering of enhanced ice flow at the bottleneck
 1506 between East and West Antarctica. *Geophysical Research Letters*, 45(10), 4899-4907.
 1507 (2018).

1508 Wolovick, M.J., Creyts, T.T., Buck, W.R., and Bell, R.E. Traveling slippery patches produce
 1509 thickness-scale folds in ice sheets, *Geophysics Research Letters*, 41, 8895–8901,
 1510 doi:10.1002/2014GL062248. (2014).

1511 Wolstencroft, M. et al. Uplift rates from a new high-density GPS network in Palmer Land
 1512 indicate significant late Holocene ice loss in the southwestern Weddell Sea. *Geophys. J. Int.*
 1513 203, 737–754 (2015).

1514 Woodward, J., Smith, A.M., Ross, N., Thoma, M., Corr, H.F.J., King, E.C., King, M.A.,
 1515 Grosfeld, K., Tranter, M., Siegert, M.J. Location for direct access to subglacial Lake
 1516 Ellsworth. *Geophysical Research Letters*, 37, L11501, doi:10.1029/2010GL042884. (2010).

1517 Wright, A.P. & Siegert, M.J. A fourth inventory of Antarctic subglacial lakes. *Antarctic*
 1518 *Science*, 24, 659-664 doi:10.1017/S095410201200048X (2012).

1519 Wright, A.P., A. M. Le Brocq, S. L. Cornford, R.G. Bingham, H.F.J. Corr, F. Ferrocchioli, T.A.
 1520 Jordan, A.J. Payne, D.M. Rippin, N. Ross and M.J. Siegert. Sensitivity of the Weddell Sea

1521 sector ice streams to sub-shelf melting and surface accumulation. *The Cryosphere*, 8, 2119-
1522 2134 doi:10.5194/tc-8-2119-2014 (2014).

1523 Wrona, T., Wolovick, M., Ferraccioli, F., Corr, H., Jordan, T. and Siegert, M.J. Position and
1524 variability of complex structures in the central East Antarctic Ice Sheet. In, Siegert, M.J.
1525 Jamieson, S.S.R. & White, D.A. (eds) *Exploration of Subsurface Antarctica: Uncovering Past*
1526 *Changes and Modern Processes*. Geological Society, London, Special Publications,
1527 461, 113-130. <https://doi.org/10.1144/SP461.12> (2018).

1528

Figure 1.

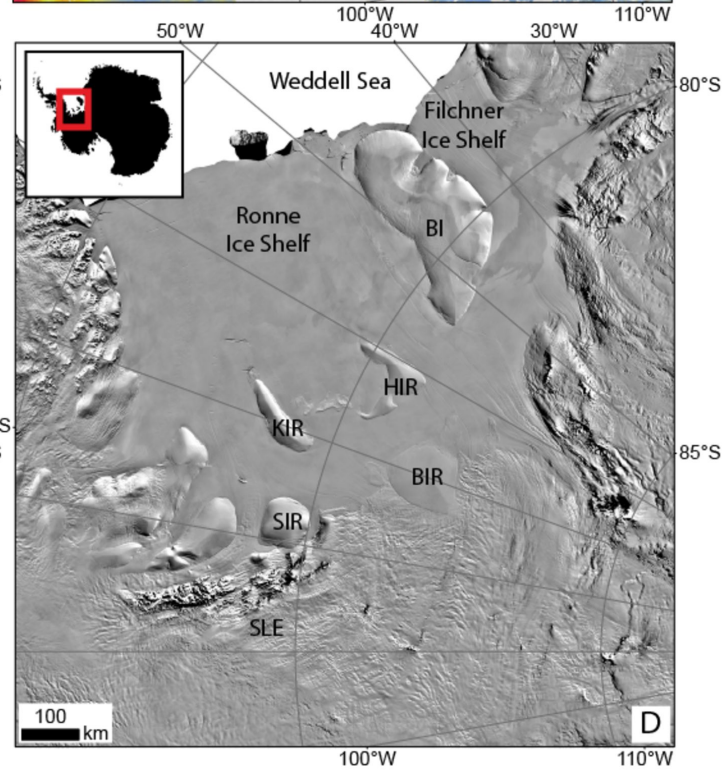
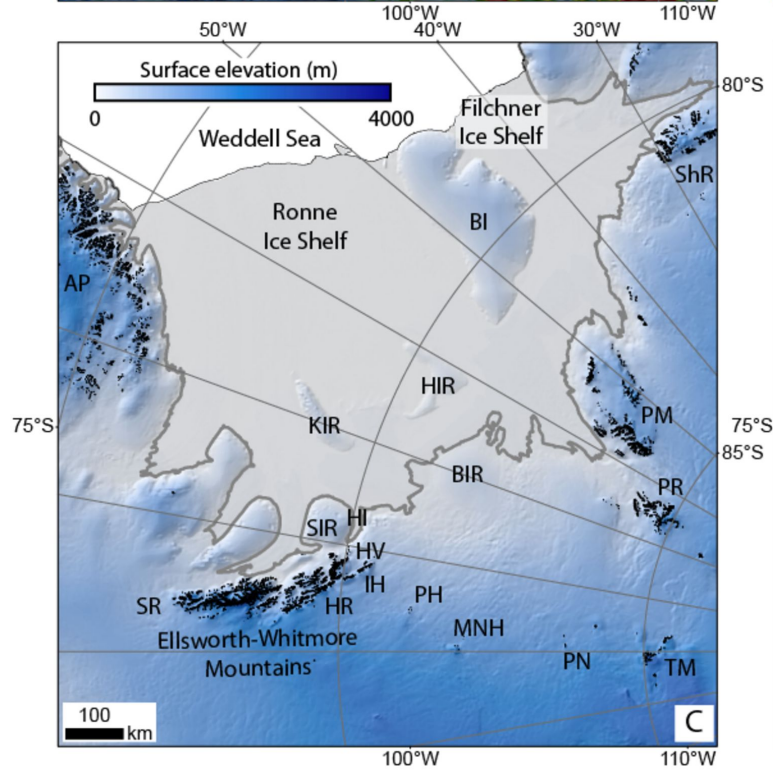
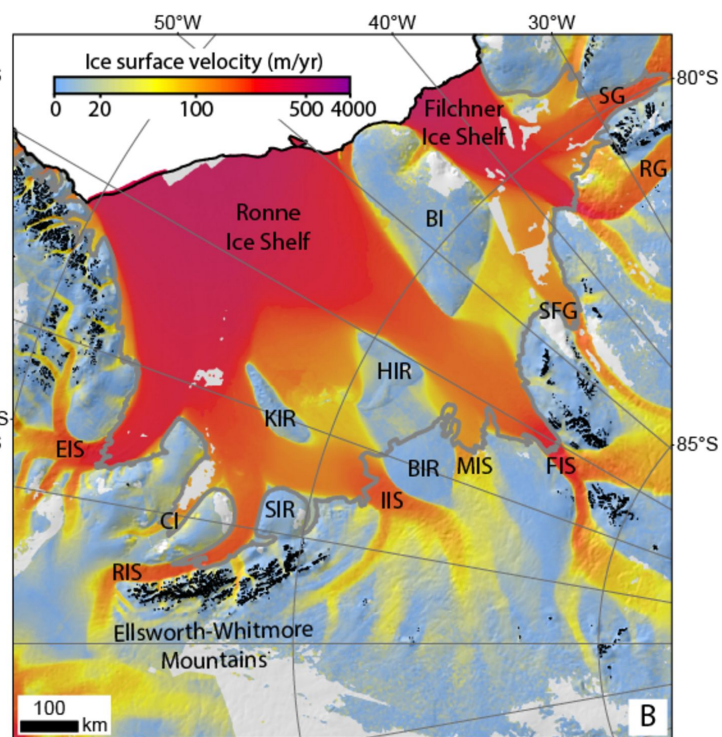
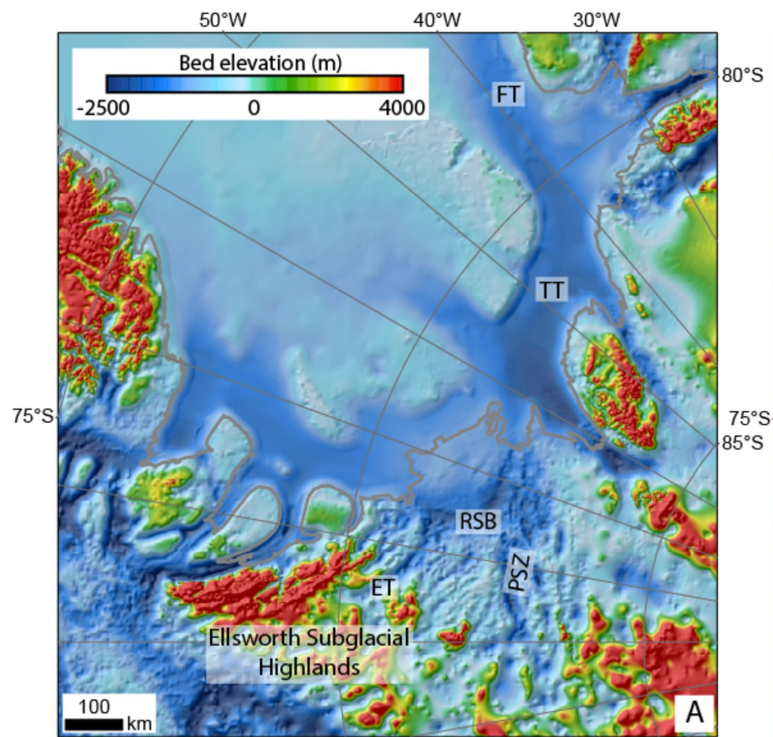


Figure 2.

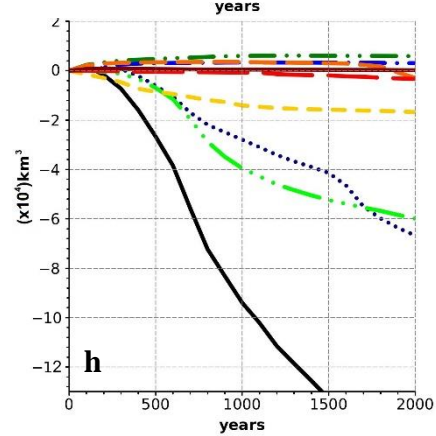
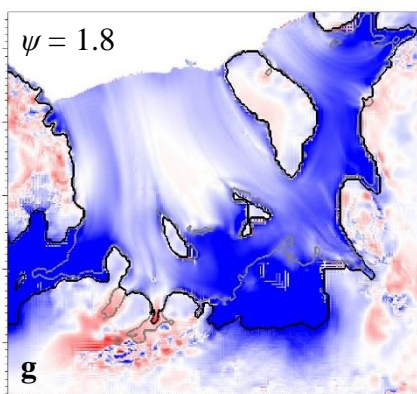
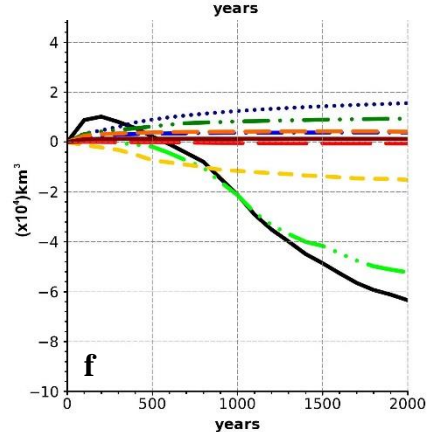
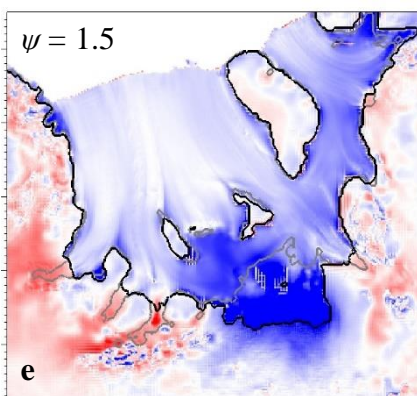
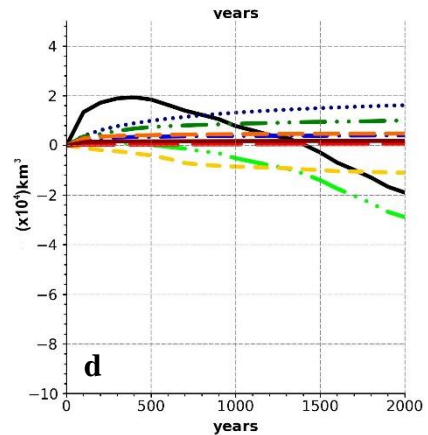
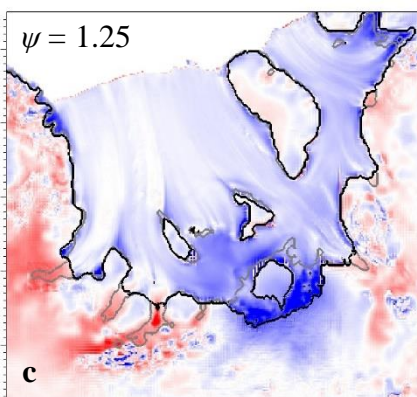
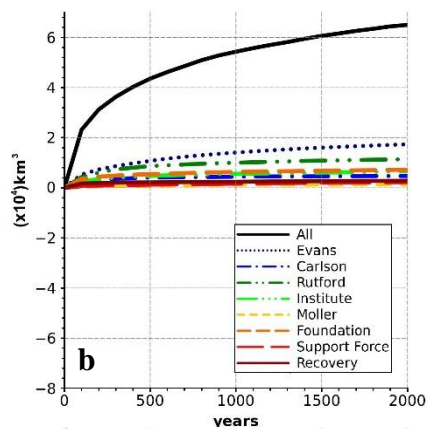
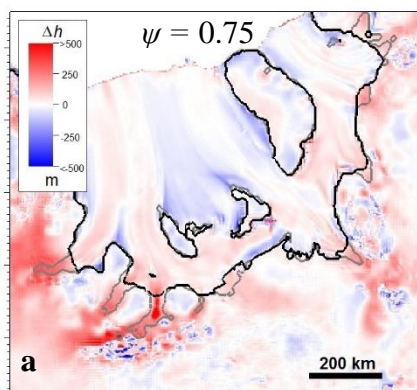


Figure 3.

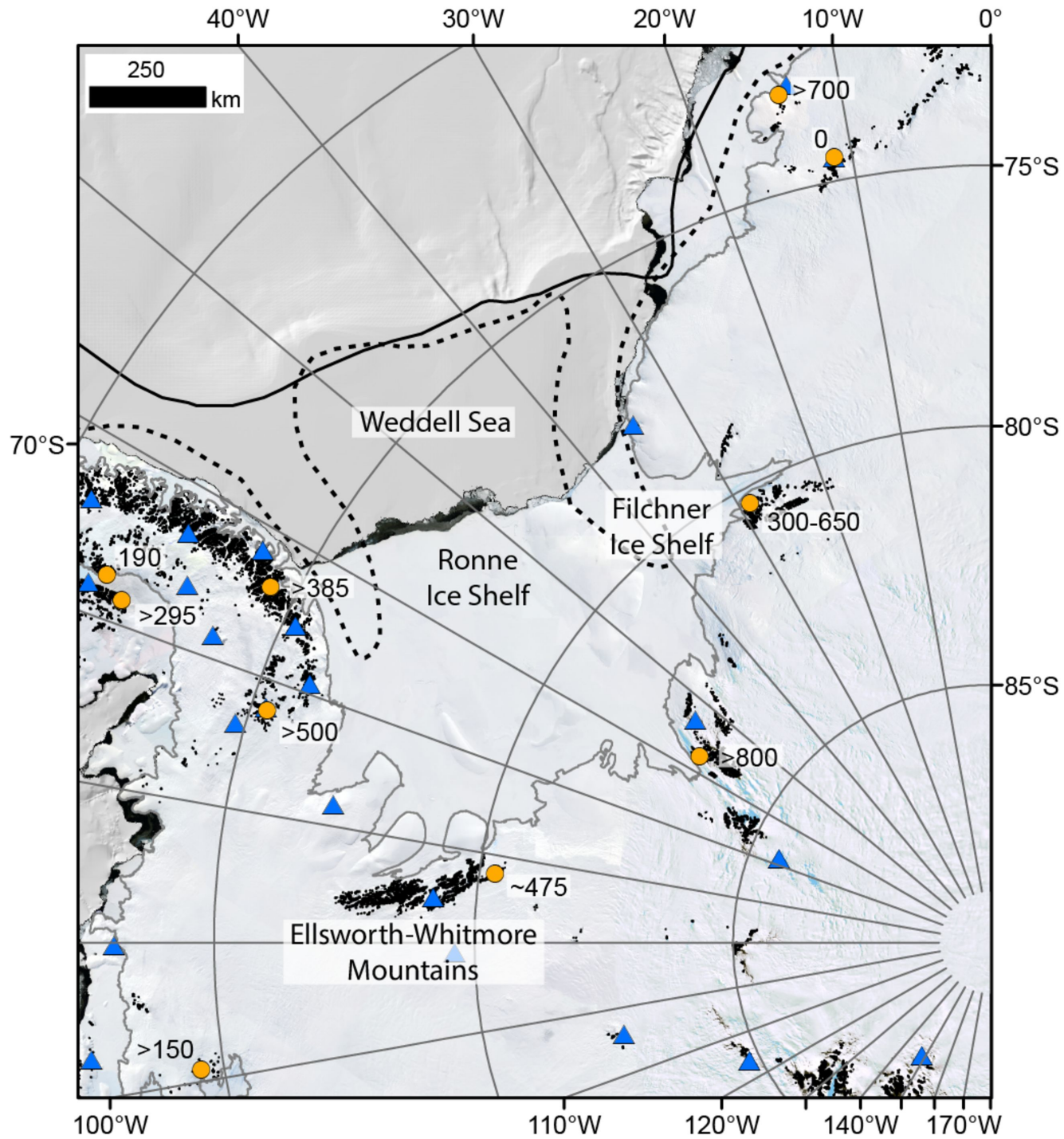


Figure 4.

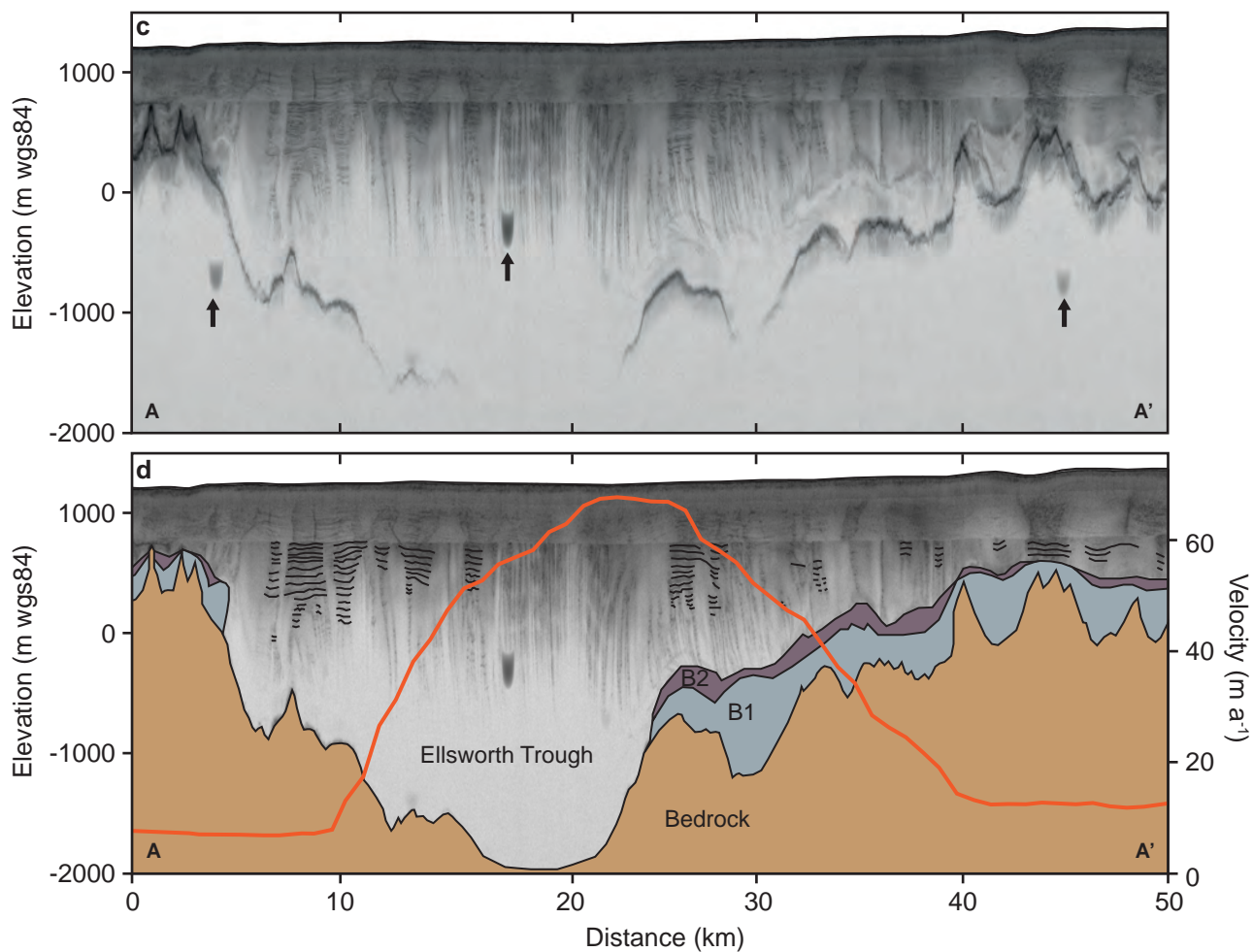
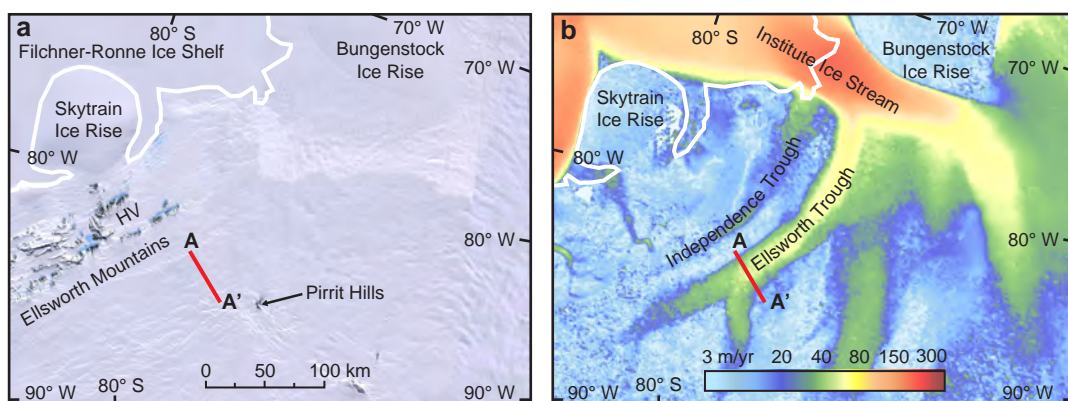


Figure 5.

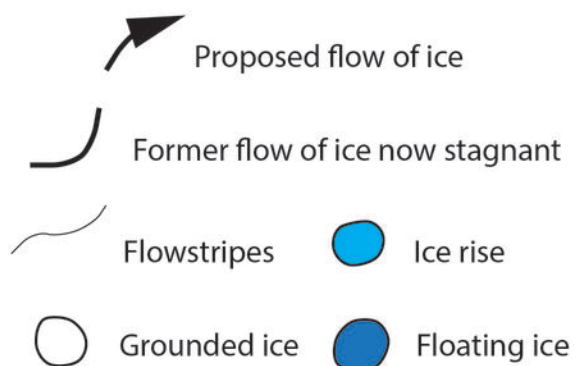
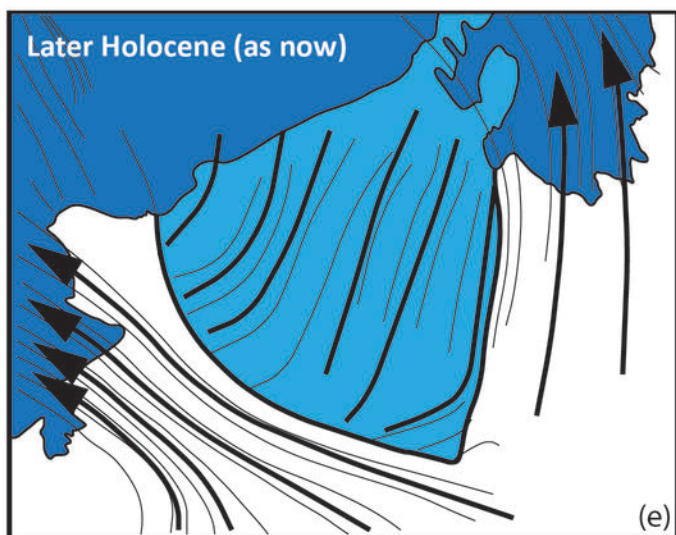
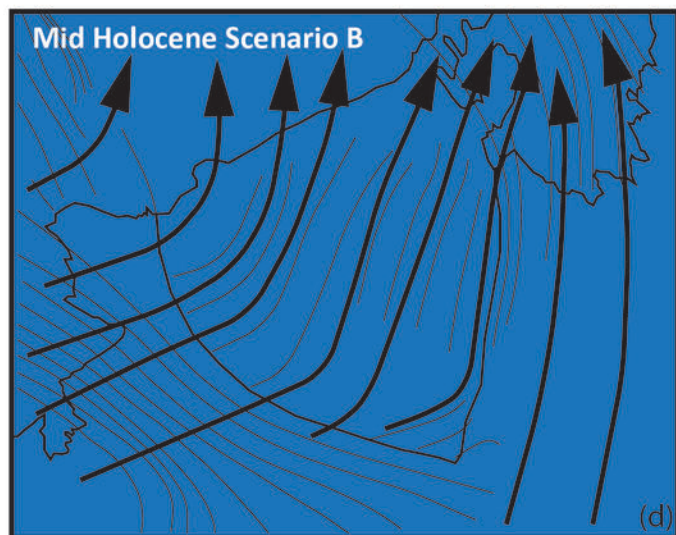
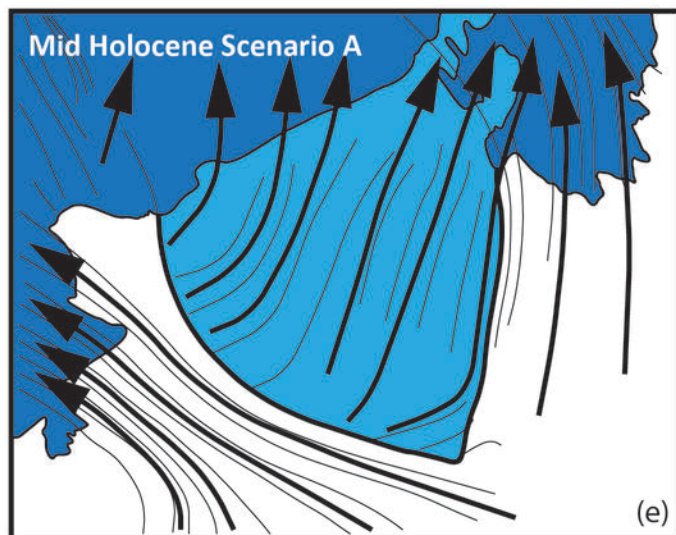
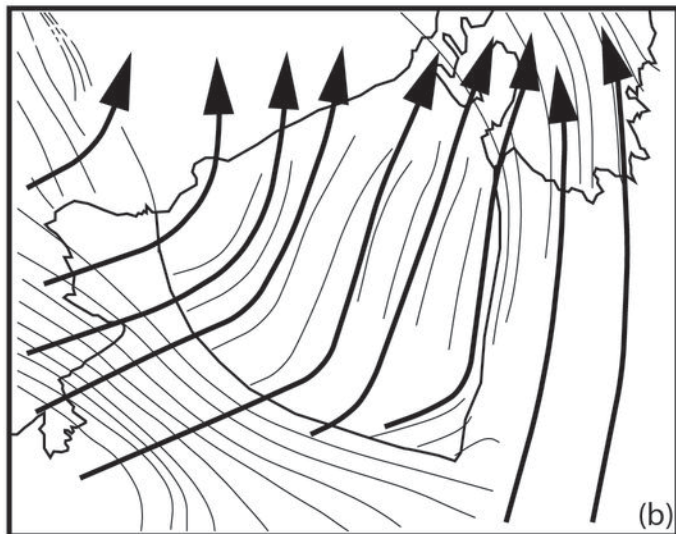
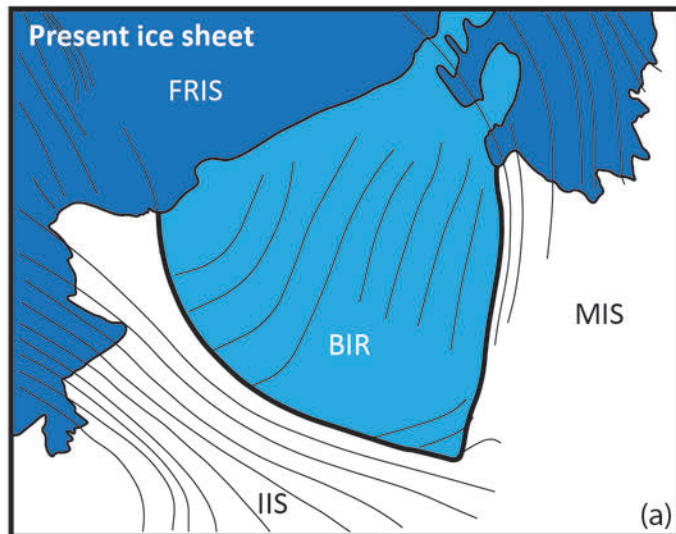


Figure 6.

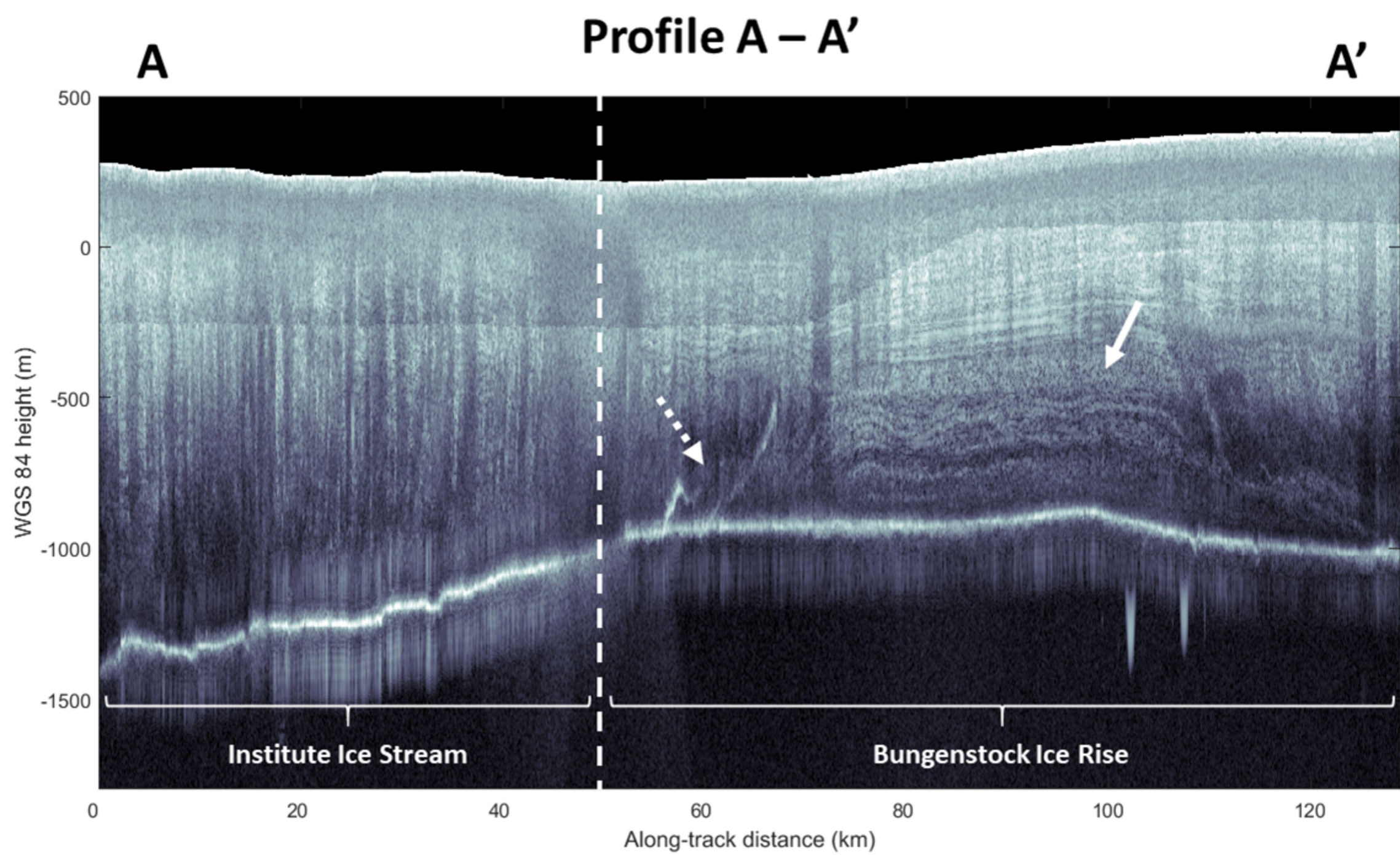
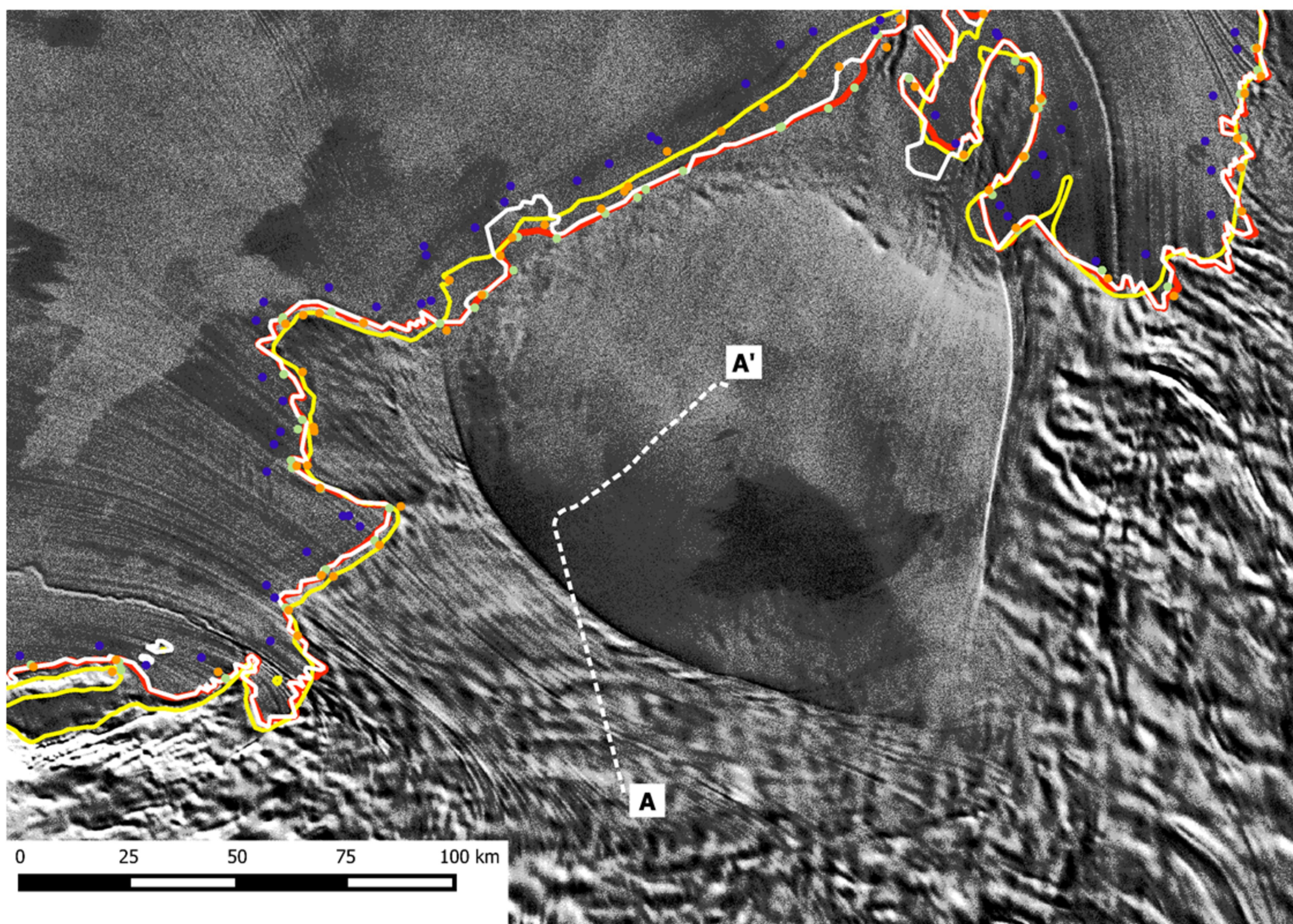


Figure 7.

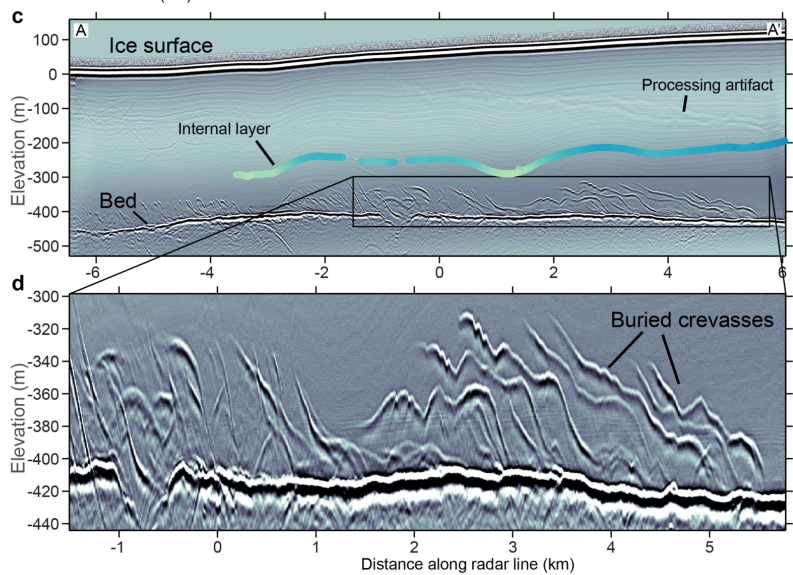
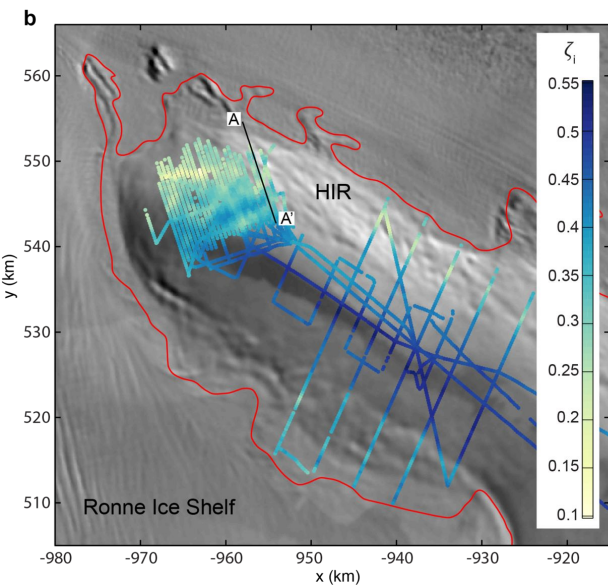
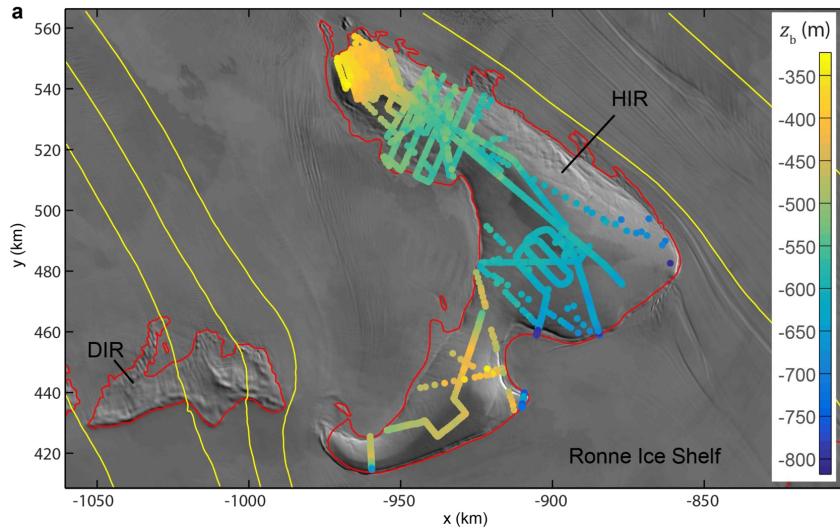


Figure 8.

Height above ice

A

Holocene

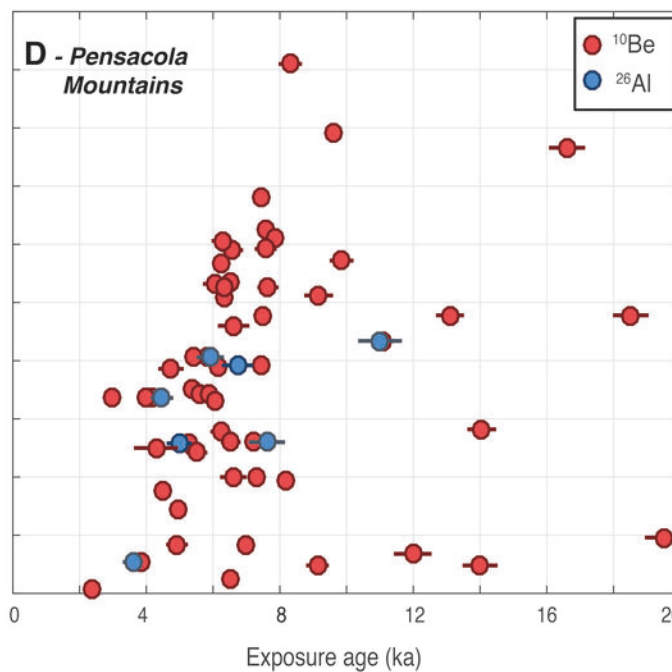
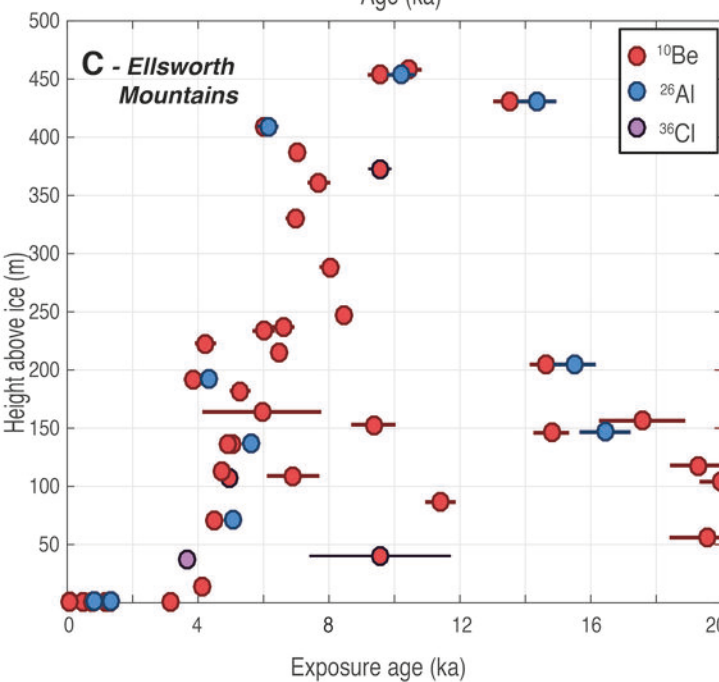
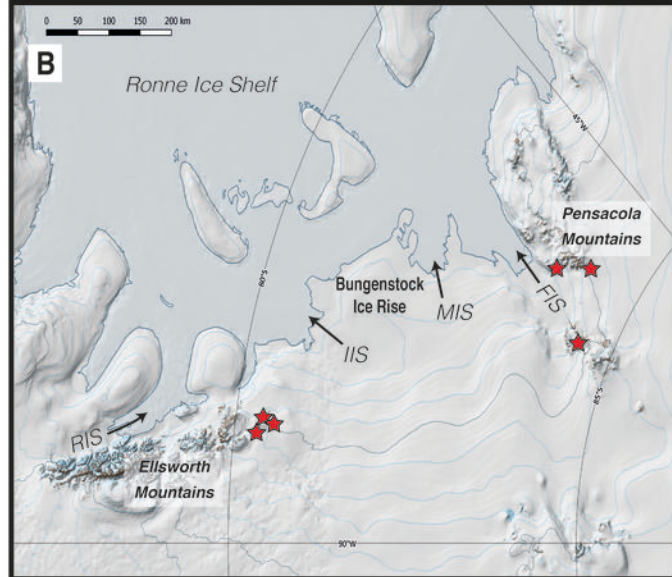
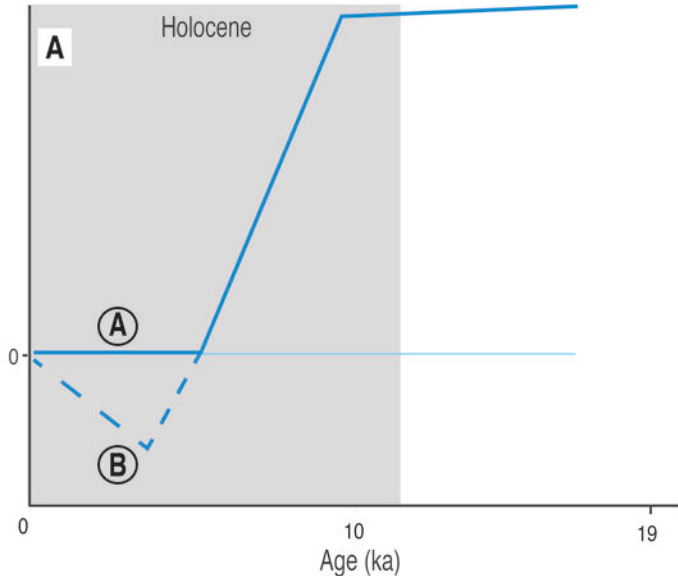


Figure 9.

